

Baryon acoustic oscillation methods for generic curvature: Application to the SDSS-III Baryon Oscillation Spectroscopic Survey

Asta Heinesen,^{a,1} Chris Blake,^b Yong-Zhuang Li,^a
David L. Wiltshire^a

^aSchool of Physical & Chemical Sciences, University of Canterbury,
Private Bag 4800, Christchurch 8140, New Zealand

^bCentre for Astrophysics & Supercomputing, Swinburne University of Technology,
P.O. Box 218, Hawthorn, VIC 3122, Australia

E-mail: asta.heinesen@pg.canterbury.ac.nz, cblake@swin.edu.au,
yong-zhuang.li@pg.canterbury.ac.nz, david.wiltshire@canterbury.ac.nz

Abstract. We develop methods for investigating baryon acoustic oscillation (BAO) features in cosmological models with non-trivial (but slowly varying) averaged spatial curvature: models that are not necessarily flat, close to flat, nor with constant spatial curvature. The class of models to which our methods apply include Lemaître-Tolman-Bondi models, modified gravity cosmologies, and inhomogeneous cosmologies with backreaction – in which we do not have a prediction of the shape of the spatial 2-point correlation function, but where we nevertheless expect to see a BAO feature in the present-day galaxy distribution, in form of an excess in the galaxy 2-point correlation function.

We apply our methods to the Baryon Oscillation Spectroscopic Survey (BOSS) dataset, investigating both the Lambda Cold Dark Matter (Λ CDM) and timescape cosmological models as case studies. The correlation functions measured in the two fiducial models contain a similarly-pronounced BAO feature. We use the relative tangential and radial BAO scales to measure the anisotropic Alcock-Paczyński distortion parameter, ϵ , which is independent of the underlying BAO preferred scale. We find that ϵ is consistent with zero in both fiducial cosmologies, indicating that models with a different spatial curvature evolution can account for the relative positions of the tangential and radial BAO scale. We validate our methods using Λ CDM mocks.

Keywords: gravity, baryon acoustic oscillations, galaxy clustering

ArXiv ePrint: [1811.11963](https://arxiv.org/abs/1811.11963)

¹Corresponding author.

1	Introduction	2
2	Theory	3
2.1	Generalising the comoving distance definition to non-FLRW space-times	3
2.2	Models under investigation	4
2.3	Alcock-Paczyński scaling	6
2.4	Overview of the timescape model	8
2.5	The Landy-Szalay estimators	10
3	Galaxy surveys, random catalogues, and mocks	12
3.1	The galaxy surveys	12
3.2	The random catalogues	13
3.3	The mocks	13
4	Empirical model for the correlation function, and extraction of the BAO characteristic scale	14
4.1	The fitting function	14
4.2	Testing on Λ CDM mocks	17
5	Data analysis	20
5.1	Isotropic fitting analysis	21
5.2	Anisotropic fitting analysis	22
6	Discussion	27
Appendix A Taylor expansion of geodesic distances		29
A.1	Spherically symmetric metrics	31
Appendix B The 2-point correlation function		32

1 Introduction

The study of baryon acoustic oscillation (BAO) features in the recent-epoch matter distribution is, together with the cosmic microwave background (CMB) and supernovae, a cornerstone of observational cosmology. In the Lambda Cold Dark Matter (Λ CDM) cosmology, sound waves in the primordial plasma, and the subsequent decoupling of photons from the baryons, produce a characteristic scale in the distribution of the baryons at the drag epoch [1, 2], which is predicted to be visible in the matter distribution of today.

The BAO feature, in the form of an excess in the spatial 2-point correlation function of the matter distribution [3, 4] was first detected in the distribution of galaxies by [5, 6] and, since then, more precisely measured by large-volume galaxy surveys such as the WiggleZ Dark Energy Survey [7] and the Baryon Oscillation Spectroscopic Survey [8]. The BAO feature has also been detected using the Lyman- α absorption line of hydrogen as a tracer of the matter distribution [9, 10]. The visibility of a characteristic scale in the 2-point matter distribution, at around the expected acoustic scale from CMB constraints [11], is a success of the Λ CDM cosmology as a self-consistent framework for the interpretation of cosmological observations.

However, as successful as the Λ CDM cosmological model might be for describing available data, it has foundational mysteries – physically unexplained dark components must account for 95% of the energy content of the universe – and observational tensions between different probes [12–16], that motivate a continued exploration of alternative models. The statistical and systematic errors in current data, and the observational degeneracy of different physical phenomena, makes it difficult to discriminate between Λ CDM and alternative cosmologies. With next-generation surveys by facilities such as the Large Synoptic Survey Telescope (LSST), Gaia, Euclid, the Dark Energy Spectroscopic Instrument (DESI) and the Square Kilometre Array (SKA), we will enter a new level of precision in data, that must be matched by theoretical precision in order to improve our understanding of the universe.

Most current analyses interpret cosmological data within the (spatially flat) Friedman-Lemaître-Robertson-Walker (FLRW) class of models. However, general relativity allows for a much richer curvature behaviour. The timescape cosmology [17, 18] and tardis cosmology [19] are phenomenological examples of models with non-FLRW spatial curvature evolution, as arises in schemes with backreaction from small-scale inhomogeneities [20, 21]. The timescape model has significantly different predictions to the spatially flat Λ CDM model for several observables, such as cosmographic relationships and redshift drift [23]. Improved data precision will allow us to discriminate between cosmological models with different spatial curvature evolution. For example, projections for the Euclid satellite show that the Λ CDM, timescape and tardis models should be observationally distinguishable: see [22], Fig. 10. Realizing such goals, however, also requires that data is reduced in as model-independent manner as possible when performing any tests of galaxy clustering, such as BAO extraction.

BAO analysis is usually performed assuming a fiducial spatially flat Λ CDM cosmology to transform data into a “comoving grid”, from which the galaxy 2-point correlation function can be estimated and the BAO scale extracted by fitting a fiducial Λ CDM power spectrum [24, 25]. Additional fiducial cosmology analysis steps, such as Λ CDM density-field reconstruction [26], are also often applied. *A priori*, results based on fiducial data-reduction procedures are not valid beyond the given fiducial model, and any extension of such results must be carefully examined for the particular class of models of interest. The extent to which the fiducial Λ CDM results can be applied when considering models with non-trivial spatial curvature is not clear, as the regime of application is usually investigated for FLRW models close to the

original fiducial cosmology.

In this paper we develop methods for using generic metrics to transform galaxy data into a correlation function. Furthermore, we propose and test an empirical fitting procedure with no model assumptions to extract a characteristic scale in the 2-point correlation function. Our fitting procedure can be applied to a large class of cosmological models. We focus on probing a statistical volume-averaged BAO feature. This does not mean that local environmental effects in the BAO feature are unexpected (see, e.g., [27–29]), but in this paper we probe the volume-averaged BAO scale for which local effects are marginalised.

We apply our new methods to the CMASS and LOWZ galaxy surveys of the Baryon Oscillation Spectroscopic Survey 12th Data Release (BOSS DR12). Testing our empirical procedure on Λ CDM BOSS mocks, we recover the BAO scale as the characteristic scale in our empirical fitting function. Our fits to the data using a Λ CDM fiducial cosmology also agree with the results of previous fiducial Λ CDM analyses [24, 25]. We then demonstrate our new methods by self-consistently re-analysing the BOSS dataset assuming the timescape cosmological model.

We summarize the structure of our paper as follows. In section 2.1 we extend the notion of FLRW comoving distances to geodesic distances on preferred spatial hypersurfaces in generic globally hyperbolic space-times in order to calculate the spatial 2-point correlation function for generic models. A restriction to spherical symmetry is then made in order to be able to split small spatial distances into angular and transverse parts, and to associate the redshift with a radial coordinate. The class of models we investigate is detailed in section 2.2, and in section 2.3 we define an Alcock-Paczyński scaling equivalent to that used in standard BAO analyses for FLRW models (see e.g., [30]). This allows us to parameterise the model cosmology in terms of an underlying “true” spherically-symmetric metric. The accuracy of the Alcock-Paczyński scaling depends on the models tested and the size of the survey domain. In section 3 we present the DR12 CMASS and LOWZ galaxy surveys, random catalogues and simulated mocks used in this analysis. In section 4.1 we propose an empirical fitting function for BAO analysis, and in section 4.2 we use the Λ CDM mocks to test that we recover the BAO scale for a Λ CDM fiducial cosmology. In section 5 we analyse the BOSS DR12 LOWZ and CMASS surveys in both the timescape and Λ CDM cosmologies. We discuss our results and possible extensions in section 6.

2 Theory

2.1 Generalising the comoving distance definition to non-FLRW space-times

In BAO analysis we consider the spatial 2-point correlation function, which describes the excess probability of two galaxies being a certain spatial distance apart as compared to a Poisson point process. We are thus concerned with the *spatial* separation of galaxies, even though we are observing galaxies from a wide range of “cosmic times” when creating our galaxy catalogues.

However, if we know the (statistical) extension of the galaxy world-lines from the cosmic time of observation, we can map the galaxy distribution on our null cone to a spatial hypersurface of reference. In FLRW cosmology this is done by tracking the galaxies through their comoving coordinates. One can then define spatial comoving distances between the galaxies at the present epoch, and recover the distances at any other reference hypersurface via multiplication by the homogeneous scale factor. For general globally hyperbolic space-times we can also track the galaxy distribution in comoving coordinates to a reference hypersurface, on

which we can compute the shortest spatial distances between galaxy pairs that are analogous to FLRW comoving separations.

We consider a globally hyperbolic space-time, and assume that the vorticity of the matter distribution in this space-time can be ignored¹, and that caustics in the matter distribution can be ignored at the coarse-graining level and over the timescale considered. The metric can then in general be written in Gaussian normal coordinates, $x^\mu = (t, x^i)$,

$$ds^2 = -\alpha^2 c^2 dt^2 + g_{ij} dx^i dx^j \quad (2.1)$$

where x^i are comoving coordinates labelling the fluid elements of the matter distribution, t labels the hypersurfaces normal to the fluid flow,² g_{ij} is the metric adapted to the hypersurfaces defined by $t = \text{constant}$, and αdt is the proper time measure on the particle worldlines.

Consider two particles (galaxies) at space-time events P_1 and P_2 with coordinates $x_1^\mu(P_1) = (t_1, x_1^i)$ and $x_2^\mu(P_2) = (t_2, x_2^i)$. We would like to define the shortest spatial distance between the two particles on a reference hypersurface $t = T$. Since the particles are by construction moving on lines of constant comoving coordinates, we can extend the particles to the reference hypersurface $t = T$. We keep the comoving coordinates x_1^i and x_2^i fixed, and consider the new space-time events $P_{1,T}$ and $P_{2,T}$ with coordinates $x_{1,T}^\mu(P_{1,T}) = (T, x_1^i)$ and $x_{2,T}^\mu(P_{2,T}) = (T, x_2^i)$. From the metric eq. (2.1) we can compute the shortest spatial distance between $P_{1,T}$ and $P_{2,T}$ on the surface $t = T$ from the geodesic equation of the adapted metric

$$ds_T^2 = g_{ij}(t = T, x^k) dx^i dx^j. \quad (2.2)$$

We denote the resulting shortest distance, $D_T(P_1, P_2)$, the Lagrangian distance between P_1 and P_2 at the reference surface $t = T$. This Lagrangian distance definition reduces to the comoving distance definition in FLRW cosmology, when the matter frame coincides with the surfaces of homogeneity and isotropy.

2.2 Models under investigation

In this section we outline the assumptions regarding the class of cosmological models for which the procedures outlined in sections 2.3 and 4.1 apply. The motivation for restricting the class of models is to be able to parameterise different cosmological models in terms of each other through an Alcock-Paczynski scaling, as outlined in section 2.3 (see e.g., [30]). We note that the results of the data analysis in the present paper can be applied *only* to the class of models discussed here.³

As in section 2.1, we consider globally hyperbolic average space-times, in which vorticity and caustics of the matter distribution can be neglected. We can write the metric in such a space-time as in eq. (2.1). We are interested in using this metric to describe the distances between galaxies within a given survey in a statistical sense. Thus, we need to write the metric in terms of coordinates (z, θ, ϕ) of the average model to which the observed redshifts, and angular positions of galaxies are mapped.

¹This assumption is made in order to define reference hypersurfaces orthogonal to the fluid frame. However, nothing prevents us from mapping the galaxy distribution to generic spatial hypersurfaces of the given space-time, allowing for a generalisation of the present procedure to the case of vorticity in the matter distribution.

²For simplicity we consider model universes where all relevant matter is in the same rest frame. This is never entirely true. The present procedure can easily be generalised to handle multicomponent fluids by simply choosing one of the fluids as a reference fluid for constructing hypersurfaces of reference.

³The standard BAO results such as [24, 25] are also limited by the regime of applicability of the AP-scaling.

Suppose that we have a set of comoving coordinates (r, θ, ϕ) , where θ and ϕ are mapped to the observed angles, and where r is a radial coordinate. For simplicity we shall assume spherical symmetry in (θ, ϕ) such that the adapted metric eq. (2.1) can be written

$$ds^2 = -\alpha(t, r)^2 c^2 dt^2 + g_{rr}(t, r) dr^2 + g_{\theta\theta}(t, r) (d\theta^2 + \cos^2(\theta) d\phi^2) \quad (2.3)$$

where $\cos^2(\theta)$ comes from the convention in the definition of the declination angle. The redshift z of radially propagating null rays, $\alpha(t, r)^2 dt^2 = g_{rr}(t, r) dr^2$, can therefore be considered as a function of either t or r (since t and r are monotonic functions of each other on radial null lines). Note that since the metric (2.3) only applies to average light propagation over large cosmic distances, z is an *average* model parameter. Although z is not directly observable, it is assumed to be a good approximation for the *mean* observed redshift. We consider universes that are overall expanding, and neglect the small scale collapse of structures that can cause the redshift to be multivalued along the null rays⁴. In such model-universes it is reasonable to assume that z is a strict monotonic function in t (and therefore also in r)⁵. In this case, we can treat z as a radial coordinate on the spatial sections $t = T$ and write the adapted metric (2.2) as⁶

$$ds_T^2 = g_{zz}(t = T, r) dz^2 + g_{\theta\theta}(t = T, r) (d\theta^2 + \cos^2(\theta) d\phi^2), \quad (2.4)$$

where⁷

$$g_{zz}(t = T, r) \equiv g_{rr}(t = T, r) \left(\frac{dr}{dz} \right)^2. \quad (2.5)$$

The BAO scale is a statistical standard ruler, and in practice the 2-point correlation function probing the BAO scale is obtained by summing over many galaxy pairs. Thus, it is reasonable to consider models with large smoothing scale compared to galaxy pair separations of order the BAO scale $\sim 100\text{Mpc}/h$. In particular, we only discuss models in which the typical pair separation of galaxies surveyed is small compared to variations of the adapted spatial metric (2.2), as detailed in appendix A. In these cases we can approximate the Lagrangian distance $D_T(P_1, P_2)$ for two galaxies with coordinates (z_1, θ_1, ϕ_1) and (z_2, θ_2, ϕ_2) separated by redshift $\delta z = z_2 - z_1$ and angle $\delta\Theta$

$$\begin{aligned} \delta\Theta &= \arccos [\sin(\theta_1) \sin(\theta_2) + \cos(\theta_1) \cos(\theta_2) \cos(\phi_2 - \phi_1)] \\ &\approx \sqrt{(\theta_2 - \theta_1)^2 + \cos^2(\bar{\theta})(\phi_2 - \phi_1)^2}, \quad \bar{\theta} = (\theta_1 + \theta_2)/2 \end{aligned} \quad (2.6)$$

⁴See section 3 of [31] for relevant calculations of mean redshift in statistically homogeneous and isotropic space-times, and section 3.2 in particular for a discussion of multivaluedness of redshift along light cones in relation to statistical homogeneity and isotropy.

⁵The monotonicity assumption is independent of the exact parameterisation, t , of the fluid-adapted foliation. Since t labels surfaces normal to the averaged fluid flow, we have $\mathbf{u} \propto \nabla t$, where \mathbf{u} is the averaged fluid 4-velocity, and t is unique up to transformations $t \rightarrow f(t)$ by a monotonic function f . Any function z that is monotonic in t will be monotonic in $f(t)$.

⁶Since the redshift, z , is only defined along the radial null geodesics it is important to realise that (2.4), (2.5) is a *projection* from the null cones onto fiducial spatial hypersurfaces, *not* a global coordinate transformation in the original space-time (2.3).

⁷In any spatially flat FLRW model, with $t = T$ corresponding to the ‘‘present time’’ hypersurface, we have $g_{rr}(t = T, r) = a(t = T)^2 = 1$ and $g_{zz}(t = T, r) = \left(\frac{dr}{dz} \right)^2 = (c/H)^2$, where $a(t)$ is the scale factor, and we have used the convention $a(t = T) = 1$.

as

$$D_T^2(P_1, P_2) \approx g_{zz}(t = T, \bar{z})(\delta z)^2 + g_{\theta\theta}(t = T, \bar{z})(\delta\Theta)^2, \quad (2.7)$$

where $\bar{z} = (z_1 + z_2)/2$ is the intermediate redshift.

The validity of the approximation of eq. (2.7) is cosmology-dependent⁸, and must be assessed for the particular class of model cosmologies of interest. In appendix A we give the explicit expansion of the geodesic path integral up to third order, and in appendix A.1 we apply our results to spherically-symmetric metrics. For the FLRW and timescape models with reasonable model parameters, we find that higher-order corrections to eq. (2.7) are of order $\lesssim 10^{-3}$ for Lagrangian galaxy separations of order 100 Mpc/h.

It will be convenient to define

$$\mu_T(P_1, P_2) = \frac{\sqrt{g_{zz}(t = T, \bar{z})(\delta z)^2}}{D_T(P_1, P_2)} \quad (2.8)$$

as the “radial fraction” of the separation. Note that such a splitting into the radial and transverse components of a geodesic distance is not meaningful for general metrics. However, when the approximation of eq. (2.6) is valid, such an Euclidean notion still applies.

Conventionally, the surface of evaluation $t = T$ is taken to be the present day. Whenever we refer to evaluation at the present day we shall omit the T subscript on eq. (2.7) and (2.8). For ease of notation the dependence on the points of the galaxies will also be implicit, and we will just write D and μ respectively.

2.3 Alcock-Paczyński scaling

In the later analysis it will be convenient to parameterise the model cosmology in terms of an unknown “true” cosmology. We will assume that the universe is well-described by a “true” metric of the form in section 2.2, and that we have a model cosmology also of the form outlined in section 2.2, but not necessarily with the same adapted metric.

We can write the model Lagrangian distance between two galaxies eq. (2.7) at mean redshift \bar{z}_i and separation δz_i , $\delta\Theta_i$ on the sky in terms of the “true” distance measures

$$\begin{aligned} (D_{T,i})^2 &\approx g_{zz}(t = T, \bar{z}_i)(\delta z_i)^2 + g_{\theta\theta}(t = T, \bar{z}_i)(\delta\Theta_i)^2 \\ &= \frac{1}{\alpha_{\parallel,i}^2} g_{zz}^{\text{tr}}(t^{\text{tr}} = T^{\text{tr}}, \bar{z}_i)(\delta z_i)^2 + \frac{1}{\alpha_{\perp,i}^2} g_{\theta\theta}^{\text{tr}}(t^{\text{tr}} = T^{\text{tr}}, \bar{z}_i)(\delta\Theta_i)^2 \end{aligned} \quad (2.9)$$

where “tr” stands for the “true” cosmology, the index i labels the galaxy pair, and

$$\alpha_{\parallel,i} \equiv \sqrt{\frac{g_{zz}^{\text{tr}}(t^{\text{tr}} = T^{\text{tr}}, \bar{z}_i)}{g_{zz}(t = T, \bar{z}_i)}}, \quad \alpha_{\perp,i} \equiv \sqrt{\frac{g_{\theta\theta}^{\text{tr}}(t^{\text{tr}} = T^{\text{tr}}, \bar{z}_i)}{g_{\theta\theta}(t = T, \bar{z}_i)}} \quad (2.10)$$

⁸The validity of the approximation relies on second order variations of the metric (curvature degrees of freedom) being small as compared to the metric and its first order variations in the adapted coordinate-system (z, θ, ϕ) over scales of the galaxy pair separations of interest (see appendix A). Examples of models with significant spatial curvature for which eq. (2.7) apply to a good approximation for galaxy pair separations of order $\sim 100\text{Mpc}/h$ are the empty Milne universe (FLRW with $\Omega_M = \Omega_\Lambda = 0$, $\Omega_k = 1$) and the timescape model, which have significant metric variations only on scales ${}^3\mathcal{R}^{-1/2} \sim c/H_0 \sim 3 \text{ Gpc}/h$ at the present epoch, where ${}^3\mathcal{R}$ is the spatial Ricci scalar of the given model.

are the Alcock-Paczyński (AP) scaling parameters. Note that we are comparing a reference hypersurface of the “true” cosmology $t^{\text{tr}} = T^{\text{tr}}$ to the reference hypersurface $t = T$ of the model cosmology, by associating points of the same observational coordinates (z, θ, ϕ) .

Each galaxy pair will be associated with its own unique scalings of eq. (2.10). For sufficiently small volumes of the galaxy survey considered, we might approximate the individual distortion parameters by one global scaling $\alpha_{\parallel}, \alpha_{\perp}$ to lowest order. This is a reasonable approximation if the survey volume has a relatively narrow redshift distribution, and if both the “true” and the model metric are slowly changing in redshift. As a rule of thumb, the narrower the redshift distribution, and the larger the curvature scales of the models of interest, the better the global scaling approximation is. In the present work we use the global AP-scaling as a rough tool for testing consistency of the investigated fiducial cosmologies, keeping in mind the limitations of this approximation.

We can define the “isotropic scaling” α and the “anisotropic scaling” ϵ

$$\alpha \equiv (\alpha_{\perp}^2 \alpha_{\parallel})^{1/3}, \quad (1 + \epsilon)^3 \equiv \frac{\alpha_{\parallel}}{\alpha_{\perp}}. \quad (2.11)$$

Such a decomposition will be useful in the following analysis, since in an isotropically-sampled galaxy distribution we expect the BAO feature to be degenerate with α and not ϵ . (See section 4.1 for explicit expressions in the context of the particular fitting function used in this analysis.) We note that α and ϵ as defined in eq. (2.11) are analogous to the AP-scaling parameters outlined in, e.g., [30], when associating g_{zz} with the inverse Hubble parameter multiplied by the speed of light c/H and $g_{\theta\theta}$ with the angular diameter distance D_A .

The isotropic scaling α describes how the volume measure of a small coordinate volume $\delta z \cos(\theta) \delta\theta \delta\phi$ differs to lowest order between the “true” and the model cosmology,

$$\alpha \approx \left(\frac{\delta V_i^{\text{tr}}(t^{\text{tr}} = T^{\text{tr}}, \bar{z}_i)}{\delta V_i(t = T, \bar{z}_i)} \right)^{1/3} = \left(\frac{g_{zz}^{\text{tr}}(t^{\text{tr}} = T^{\text{tr}}, \bar{z}_i) (g_{\theta\theta}^{\text{tr}}(t^{\text{tr}} = T^{\text{tr}}, \bar{z}_i))^2}{g_{zz}(t = T, \bar{z}_i) (g_{\theta\theta}(t = T, \bar{z}_i))^2} \right)^{1/6} \quad (2.12)$$

with

$$\delta V_i(t = T, \bar{z}_i) \equiv \sqrt{\det(g)}(t = T, \bar{z}_i) \delta z \delta\theta \delta\phi, \quad (2.13)$$

where $\det(g)$ is the determinant of the spatial metric (2.4) in the coordinate basis (z, θ, ϕ) .

It will prove convenient to parameterise α and ϵ of two model cosmologies in terms of the relative transverse and radial distance measures of the models

$$\begin{aligned} \alpha_1 &= \alpha_2 \left(\frac{g_{2,zz}(t_2 = T_2, \bar{z})}{g_{1,zz}(t_1 = T_1, \bar{z})} \right)^{1/6} \left(\frac{g_{2,\theta\theta}(t_2 = T_2, \bar{z})}{g_{1,\theta\theta}(t_1 = T_1, \bar{z})} \right)^{1/3} \\ \epsilon_1 &= (1 + \epsilon_2) \left(\frac{g_{2,zz}(t_2 = T_2, \bar{z})}{g_{1,zz}(t_1 = T_1, \bar{z})} \right)^{1/6} \left(\frac{g_{2,\theta\theta}(t_2 = T_2, \bar{z})}{g_{1,\theta\theta}(t_1 = T_1, \bar{z})} \right)^{-1/6} - 1. \end{aligned} \quad (2.14)$$

Knowing α (ϵ) within a reference/fiducial cosmology, we can calculate α (ϵ) within a different cosmology from the known model distance measures using the identity in eq. (2.14).

From the assumption of slowly varying α_{\perp} and α_{\parallel} over the survey volume we can approximate

$$(D_{T,i})^2 \approx \frac{1}{\alpha_{\perp}^2} g_{zz}^{\text{tr}}(t^{\text{tr}} = T^{\text{tr}}, \bar{z}_i) (\delta z_i)^2 + \frac{1}{\alpha_{\perp}^2} g_{\theta\theta}^{\text{tr}}(t^{\text{tr}} = T^{\text{tr}}, \bar{z}_i) (\delta\Theta_i)^2, \quad (2.15)$$

which we can invert to $D_{T^{\text{tr}}}$ approximated in terms of D_T , μ_T , and the global Alcock-Paczyński scaling parameters α_{\parallel} , α_{\perp} .

$$\begin{aligned}
(D_{T^{\text{tr}},i}^{\text{tr}})^2 &\approx g_{zz}^{\text{tr}}(t^{\text{tr}} = T^{\text{tr}}, \bar{z}_i)(\delta z_i)^2 + g_{\theta\theta}^{\text{tr}}(t^{\text{tr}} = T^{\text{tr}}, \bar{z}_i)(\delta\Theta_i)^2 \\
&\approx \alpha_{\parallel}^2 g_{zz}(t = T, \bar{z}_i)(\delta z_i)^2 + \alpha_{\perp}^2 g_{\theta\theta}(t = T, \bar{z}_i)(\delta\Theta_i)^2 \\
&= \alpha_{\perp}^2 (D_{T,i})^2 \left(1 + \left(\frac{\alpha_{\parallel}^2}{\alpha_{\perp}^2} - 1 \right) \mu_{T,i} \right) \\
&= \alpha^2 (D_{T,i})^2 \left(\frac{\alpha_{\perp}}{\alpha_{\parallel}} \right)^{2/3} \left(1 + \left(\frac{\alpha_{\parallel}^2}{\alpha_{\perp}^2} - 1 \right) \mu_{T,i}^2 \right),
\end{aligned} \tag{2.16}$$

where the definition of μ_T in eq. (2.8) has been used. Similarly we have for μ^{tr}

$$\mu_{T^{\text{tr}},i}^{\text{tr}} = \frac{\sqrt{g_{zz}^{\text{tr}}(t^{\text{tr}} = T^{\text{tr}}, \bar{z}_i)(\delta z_i)^2}}{D_{T,i}^{\text{tr}}} \approx \frac{\alpha_{\parallel}}{\alpha_{\perp}} \mu_{T,i} \frac{1}{\sqrt{1 + \left(\frac{\alpha_{\parallel}^2}{\alpha_{\perp}^2} - 1 \right) \mu_{T,i}^2}}. \tag{2.17}$$

2.4 Overview of the timescape model

In the present analysis we apply our methods to the spatially flat Λ CDM and the timescape cosmologies. Both models are part of the class described in section 2.2, and we can therefore test them with the procedures outlined in this paper.

The timescape cosmology [17, 18] is a model which invokes non-trivial backreaction of inhomogeneous structures on $\lesssim 100$ Mpc/ h scales on the average expansion of the universe. In particular, Einstein’s equations are not taken to govern a global background metric, rather matter and geometry couple *locally*, allowing for non-trivial curvature evolution. In the timescape model the early universe is close to critical density (and well-approximated by a spatially flat FLRW geometry) and evolves into a void-dominated present day universe of average negative spatial curvature. Typical observers in the timescape model have a mass-biased view of the universe, as they are located in gravitationally-bound structures which are overdense with respect to the average density of the universe. For a review of the timescape model and its observable consequences, see [32].

The timescape model and spatially Λ CDM model have the same number of free parameters. In both cases, the main features of the late epoch universe are determined by two independent parameters, which can be thought of as the Hubble parameter and a matter density parameter. However, in the timescape case, on account of inhomogeneities, not every observer is the same average observer with identical clocks and rulers. There are “bare” and “dressed” versions of each parameter – the bare ones referring to volume averages of the small scale Einstein equations which best describes average cosmic evolution [20], and the dressed ones to observers like ourselves in gravitational bound systems and the measurements on our past light cone in terms of our rulers and clocks [17]. The dressed parameters are the observationally relevant ones for model comparisons.

In the present paper we aim to demonstrate feasibility of the method, by making just one choice of the timescape dressed matter density parameter, equal to that of the Λ CDM matter density parameter, $\Omega_{M0} = 0.3$ at the present epoch. However, it should be stressed that dressed parameter in the timescape case does not enter any Friedmann-like Hamiltonian constraint equation. Furthermore, the value chosen is a reasonable one in the timescape case [33, 34], but not singled out as a best fit in other tests [35].

In the timescape “tracking limit” [23] applicable to redshifts $z \lesssim 10$, the adapted metric (2.4) of the timescape model is given by an exact solution [18]

$$\sqrt{g_{\theta\theta}(t = t_0, r(t))} = (1 + z)ct^{2/3} (\mathcal{F}(t_0) - \mathcal{F}(t)), \quad \sqrt{g_{zz}(t = t_0, r(t))} = \frac{c}{H}, \quad (2.18)$$

where the position $r(t)$ of sources on radial null rays is parameterised in terms of the volume–average time parameter at emission, t_0 denotes the present epoch value of t ,

$$H(t) = \frac{3(2t^2 + 3bt + 2b^2)}{t(2t + 3b)^2}, \quad (2.19)$$

is the dressed Hubble parameter relevant for all observational measures in this paper,

$$\mathcal{F}(t) = 2t^{1/3} + \frac{b^{1/3}}{6} \ln \left(\frac{(t^{1/3} + b^{1/3})^2}{t^{2/3} - b^{1/3}t^{1/3} + b^{2/3}} \right) + \frac{b^{1/3}}{\sqrt{3}} \tan^{-1} \left(\frac{2t^{1/3} - b^{1/3}}{\sqrt{3}b^{1/3}} \right), \quad (2.20)$$

$b \equiv 2(1 - f_{v0})(2 + f_{v0})/[9f_{v0}\bar{H}_0]$, $\bar{H}_0 = 2(2 + f_{v0})H_0/(4f_{v0}^2 + f_{v0} + 4)$ is the “bare Hubble constant”, $H_0 = H(t_0)$ the “dressed Hubble constant”, and $f_{v0} = f_v(t_0)$ the present epoch value of the void volume fraction. In the timescape model the void volume fraction,

$$f_v(t) = \frac{3f_{v0}\bar{H}_0t}{3f_{v0}\bar{H}_0t + (1 - f_{v0})(2 + f_{v0})}, \quad (2.21)$$

is a parameter which arises in the Buchert average [20]. The dressed Ω_M parameter is not a natural timescape parameter but is constructed to take values similar to the Λ CDM case, being given by $\Omega_M = \frac{1}{2}(1 - f_v)(2 + f_v)$ with inverse $f_v = \frac{1}{2}[-1 + \sqrt{9 - 8\Omega_M}]$. An important feature of the timescape model, crucial to inferring late–epoch apparent acceleration, is that the statistical time parameter t is *not* the observed expansion age. Rather, this is given by

$$\tau = \frac{2}{3}t + \frac{2(1 - f_{v0})(2 + f_{v0})}{27f_{v0}\bar{H}_0} \ln \left(1 + \frac{9f_{v0}\bar{H}_0t}{2(1 - f_{v0})(2 + f_{v0})} \right) \quad (2.22)$$

in the tracking limit. The observed redshift then also reads

$$z + 1 = \frac{2^{4/3}t^{1/3}(t + b)}{f_{v0}^{1/3}\bar{H}_0t(2t + 3b)^{4/3}}. \quad (2.23)$$

For a derivation and discussion of the above results, see [23].

Figure 1 shows $\sqrt{g_{\theta\theta}}$ and $\sqrt{g_{zz}}$ of eq. (2.4) for the timescape and Λ CDM models with $\Omega_{M0} = 0.3$ relative to the empty universe. The same global Hubble parameter H_0 is assumed for all three models. Since $d_A \equiv \sqrt{g_{\theta\theta}(t = t_0, r(t))}/(1 + z)$ is the angular diameter distance, while $d_H \equiv \sqrt{g_{zz}(t = t_0, r(t))}/(1 + z)$ represents the projected radial proper distance between two particles separated by a small distance δz in redshift, these quantities represent the standard angular and radial distance measures.

The timescape model redshift–distance relation is closer to that of the empty universe than to Λ CDM for redshifts $z \lesssim 1$ ⁹. While the timescape model distance measures are within

⁹For high redshifts the timescape model expansion history is closer to a FLRW model containing the usual matter and radiation species. Its distance–redshift relation effectively interpolates between those of Λ CDM models with different values of Ω_{M0} and $\Omega_{\Lambda0}$ at different redshifts [23, 32].

$\sim 2\%$ of the empty universe case, the Λ CDM model differs from the empty universe by up to $\sim 15\%$ in the redshift range $0.15 \leq z \leq 0.7$.¹⁰ The low-redshift proximity of the timescape model expansion history to that of the empty universe reflects the late-epoch volume dominance of voids relative to gravitationally-bound structures, which in the timescape model gives rise to a present-day on average negatively-curved universe. Given this comparison, BOSS large-scale structure data has the potential to distinguish between these scenarios.

The timescape model is currently much less experimentally constrained than the Λ CDM model [33, 34], since a perturbation theory describing structure formation within the timescape model has yet to be developed. As a consequence CMB constraints on the BAO scale are much less precise for timescape as compared to Λ CDM. (One can fit the angular positions of the acoustic peaks CMB using conservative priors for the baryon-to-photon ratio, following an equivalent procedure to that described in appendix D of [35].) This makes the ϵ parameter the most powerful discriminator between the timescape model and Λ CDM, in the context of the present analysis.

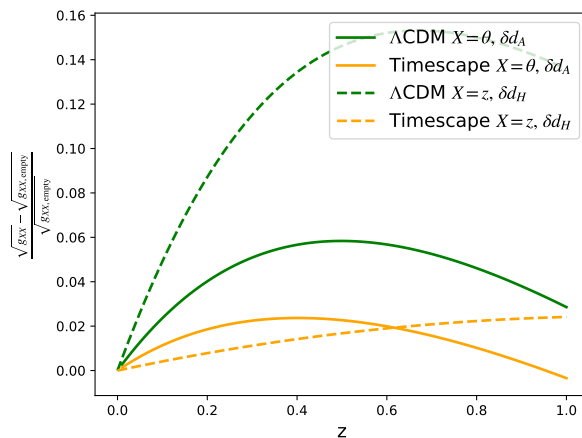


Figure 1: Λ CDM $\Omega_{M0} = 0.3$ and timescape dressed $\Omega_{M0} = 0.3$ radial and transverse distance measures, relative to the empty universe distance measures, as a function of redshift z . The axis $(\sqrt{g_{XX}} - \sqrt{g_{XX,empty}}) / \sqrt{g_{XX,empty}}$ represents the fractional difference of the angular diameter distance and radial Hubble distances for Λ CDM and timescape relative to an empty universe for an observer at the present epoch, assuming the same value of the Hubble parameter for all three models. I.e., when $X = \theta$ it corresponds to $\delta d_A \equiv (d_A - d_{A,empty}) / d_{A,empty}$ and when $X = z$ it corresponds to $\delta d_H \equiv (H^{-1} - H_{empty}^{-1}) / H_{empty}^{-1}$.

2.5 The Landy-Szalay estimators

The 2-point correlation function in cosmology (see for example [36]) describes the excess in correlation between structure in a spatial section of the universe, relative to the case in which matter is distributed according to an uncorrelated Poisson process. Thus the 2-point correlation function describes characteristic scales in the matter distribution.

¹⁰These percentage estimates would in general change for distances measured in units of Mpc (rather than units of Mpc/h) for reasonable values of H_0 of the individual models. Typical values of H_0 for the timescape model are around 10% smaller than for the Λ CDM model.

The spatial 2-point correlation function is defined as

$$\xi(X, Y) = \frac{f(X, Y)}{f(X)f(Y)} - 1 \quad (2.24)$$

where $f(X, Y)$ is the ensemble probability density of finding two galaxies at points X and Y , and $f(X)$ is the uncorrelated probability density of finding a galaxy at point X . By assuming that the galaxy distribution is well-described by a homogeneous and isotropic point process, eq. (2.24) reduces to

$$\xi(D) = \frac{f(D)}{f_{\text{Poisson}}(D)} - 1, \quad (2.25)$$

where D is the Lagrangian distance of the “true” underlying metric between the points X, Y defined in section 2.1, $f(D)$ represents the probability density of finding two objects with the mutual distance D , and $f_{\text{Poisson}}(D)$ represents the analogous probability density in the uncorrelated case. Note that we can define a correlation function with a similar form to eq. (2.25) for an inhomogeneous and anisotropic point process by marginalising over the position and direction degrees of freedom in $f(X, Y)$ (see appendix B). For a given spherically-symmetric metric, where in addition to the Lagrangian distance D we can define the radial fraction of the separation μ (see section 2.2), it will be convenient to define the correlation function analogous to eq. (2.25),

$$\xi(D, \mu) = \frac{f(D, \mu)}{f_{\text{Poisson}}(D, \mu)} - 1, \quad (2.26)$$

parameterised by μ and D . (See appendix B for details.)

Various estimators of the 2-point correlation function have been tested within Λ CDM [37]. An efficient estimator is found to be the Landy-Szalay (LS) estimator [38]

$$\hat{\xi}_{LS}(D, \mu) = \frac{DD(D, \mu) + RR(D, \mu) - 2DR(D, \mu)}{RR(D, \mu)}, \quad (2.27)$$

where DD is the binned normalised number count

$$DD(D, \mu) = \frac{1}{N_D(N_D - 1)} \sum_{a,b}^{N_D} \mathbb{1}_{D \pm \Delta D}(D(x_a^i, x_b^i)) \mathbb{1}_{\mu \pm \Delta \mu}(\mu(x_a^i, x_b^i)) \quad (2.28)$$

over galaxies in the survey, where N_D is the total number of galaxies, and ΔD and $\Delta \mu$ are the binning size, and $\mathbb{1}_A(y)$ is the indicator function, having the value 1 for $y \in A$ and 0 for $y \notin A$. RR is defined in the same way

$$RR(D, \mu) = \frac{1}{N_R(N_R - 1)} \sum_{a,b}^{N_R} \mathbb{1}_{D \pm \Delta D}(D(x_a^i, x_b^i)) \mathbb{1}_{\mu \pm \Delta \mu}(\mu(x_a^i, x_b^i)), \quad (2.29)$$

except that the sum is now over N_R artificial galaxies in a random Poisson catalogue, designed to match the galaxy density of the galaxy survey. We also define DR , the normalised cross pair-count between the galaxy catalogue and the random sample, by

$$DR(D, \mu) = \frac{1}{N_D N_R} \sum_a^{N_D} \sum_b^{N_R} \mathbb{1}_{D \pm \Delta D}(D(x_a^i, x_b^i)) \mathbb{1}_{\mu \pm \Delta \mu}(\mu(x_a^i, x_b^i)) \quad (2.30)$$

We will use the LS estimator (2.27) to estimate the underlying 2-point correlation function in this paper. It will be convenient to average this estimator in μ to obtain the wedge LS estimator,

$$\hat{\xi}_{LS[\mu_1, \mu_2]}(D) = \frac{1}{\mu_2 - \mu_1} \int_{\mu_1}^{\mu_2} d\mu \hat{\xi}_{LS}(D, \mu). \quad (2.31)$$

We define the isotropic wedge $\hat{\xi}(D)$, the transverse wedge $\hat{\xi}_\perp(D)$ and radial wedge $\hat{\xi}_\parallel(D)$ estimator as respectively

$$\hat{\xi}(D) \equiv \hat{\xi}_{LS[0,1]}(D), \quad \hat{\xi}_\perp(D) \equiv \hat{\xi}_{LS[0,0.5]}(D), \quad \hat{\xi}_\parallel(D) \equiv \hat{\xi}_{LS[0.5,1]}(D) \quad (2.32)$$

where we have dropped the subscript LS.

3 Galaxy surveys, random catalogues, and mocks

In this section we describe the datasets (observed and simulated) used in this analysis. Since the 2-point correlation function is defined as an excess probability of the correlation of galaxies compared to an unclustered Poisson distribution, we also use a random catalogue to construct the Landy-Szalay estimators (2.32). We use mock catalogues to test our analysis methods in a fiducial Λ CDM cosmology, and to estimate the covariance of our measurements.

3.1 The galaxy surveys

The Sloan Digital Sky Survey (SDSS) III [39] is a large spectroscopic redshift survey performed at the Apache Point Observatory in New Mexico. SDSS contains the Baryon Oscillation Spectroscopic Survey (BOSS) [40] of Luminous Red Galaxies (LRGs), which constitutes the current largest-volume map of large-scale structure, spanning the approximate redshift range $0.1 \leq z \leq 0.7$ across 10,000 deg^2 of sky. Different colour and magnitude cuts are used to select homogeneous galaxy types across redshift ranges $0.15 \leq z \leq 0.43$ (the LOWZ sample) and $0.43 \leq z \leq 0.7$ (the CMASS sample). The samples are split into disconnected sub-surveys containing the galaxies from the North Galactic Cap (NGC) and South Galactic Cap (SGC).

We use the BOSS Data Release 12 (DR12) [41] in this analysis. Each of the galaxies is labelled by observed coordinates (z, θ, ϕ) , where z is the observed redshift, θ is the angle of declination and ϕ is the angle of right ascension. The redshift distribution of the surveys is shown in figure 2. The total number of galaxies contained in our selected redshift intervals is 361,762 for LOWZ and 777,202 for CMASS.

We do *not* use a reconstruction procedure of peculiar motions of galaxies such as the one described in [26]. Such a procedure reconstructs the displacements of galaxies relative to a Λ CDM background based on the density field of the survey, using the relation between the linear density field and velocity fields in Λ CDM perturbation theory. Such a perturbation theory has not yet been developed for the timescape cosmology, so we do not apply it in our analysis.

In computing the spatial 2-point correlation function, we make use of the cosmology-independent ‘‘total galaxy weights’’ (or completeness weights) described by [42]. These weights are designed to account for observational biases, in order to make the observed galaxy distribution an unbiased estimate of the underlying galaxy distribution. For example, neighbours to galaxies for which redshift determination failed are up-weighted in order to compensate for the missing galaxy in the sample. We do not use Feldman, Kaiser & Peacock (FKP) weights

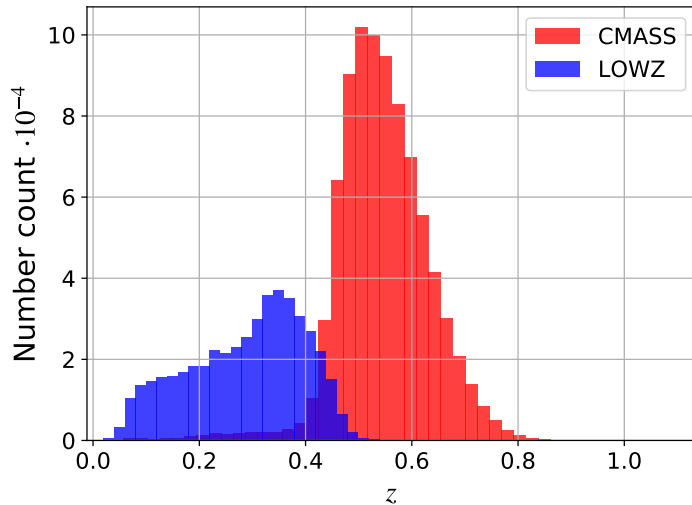


Figure 2: Redshift distribution of CMASS (red) and LOWZ (blue).

(see [42, 43]), since they are derived in the context of a fiducial cosmological model. However, the application of FKP weights does not significantly affect acoustic peak measurements in BOSS.

3.2 The random catalogues

We use random catalogues generated from the CMASS and LOWZ galaxy distributions as described by [42]. The random catalogues are generated independently of a cosmological model and are based solely on the distribution of the galaxies in observed coordinates (z, θ, ϕ) . The random catalogue uniformly samples the angular coverage of the data, and random redshifts are assigned from the redshift probability distribution of the survey. We use a random catalogue 10 times the size of the given galaxy catalogue or mock.

3.3 The mocks

The errors in the correlation function used in BAO analysis can be estimated in the context of a fiducial Λ CDM cosmology using theory or simulations. Alternatively, non-parametric methods such as jack-knife estimation can be applied.

The assumption of a fiducial cosmology in error analysis is not satisfying from the point of view of investigating a broader class of models than the fiducial cosmology. However, in practice non-parametric methods are hard to implement, as the assumptions underlying them cannot be satisfied for current galaxy surveys. To apply jack-knife variance estimation we must be able to divide our sample into a (large) number of subsamples that are well approximated as resulting from identical and independent probability distributions, i.e., we must be able to view the regions as realisations of an ensemble. Furthermore, jack-knife regions must be sufficiently large to contain enough galaxy pairs separated by the relevant scales, which conflicts with the requirement that the number of jack-knife regions must be sufficiently large to allow an accurate inverse covariance matrix to be constructed.

We instead use the Quick Particle Mesh (QPM) mocks as described in detail in [44] for error analysis. These mocks are based on Λ CDM N -body simulations, and are generated

specifically for the BOSS clustering analysis. The number density in the mock catalogues is designed to match the observed galaxy number density of the BOSS catalogues, and to follow the radial and angular selection functions of BOSS. The fiducial Λ CDM cosmology of the QPM simulations is

$$\Omega_{M0} = 0.29, \quad \Omega_{\Lambda0} = 0.71, \quad \Omega_{b0} = 0.048, \quad \sigma_8 = 0.8, \quad h = 0.7, \quad (3.1)$$

where Ω_{M0} , $\Omega_{\Lambda0}$ and Ω_{b0} are the present epoch matter density parameter, dark energy density parameter, and baryonic matter density parameter respectively, σ_8 is the root mean square of the linear mass fluctuations at the present epoch averaged at scales $8 \text{ Mpc}/h$ given by the integral over the Λ CDM power spectrum, and $H_0 = 100 h \text{ km/s/Mpc}$ is the Hubble parameter evaluated at the present epoch. The sound horizon at the drag epoch within this model is $r_s = 103.05 \text{ Mpc}/h$.

There are 1000 QPM mocks available. We use all of these to construct an approximate covariance matrix of the measured galaxy correlation function. Furthermore, we use these mocks to test how well our empirical procedure can recover the input acoustic scale and the anisotropic distortion in the fiducial Λ CDM cosmology with parameters (3.1).

4 Empirical model for the correlation function, and extraction of the BAO characteristic scale

Conventional Λ CDM BAO fitting procedures [24, 25] involve the construction of a template power spectrum model motivated by Λ CDM perturbation theory. We cannot necessarily apply these techniques in more general cosmological models. In this section we therefore develop an empirical approach for fitting the baryon acoustic oscillation feature in models with non-trivial curvature, where we do not have a model for the shape of the correlation function, but where we nevertheless expect a characteristic scale in the matter distribution to be sourced from early-universe oscillations of the baryonic plasma.

In our analysis we will leave the Hubble constant free to vary and extract the BAO scale in units Mpc/h , rather than fixing h independently to some particular value. Our key fitted parameter, ϵ , is dimensionless and independent of H_0 . In future analysis we aim to obtain independent constraints on both Ω_{M0} and H_0 from joint BAO and CMB observations; Ω_{M0} is just fixed in the present paper to develop the methodology.

4.1 The fitting function

The simplest model-independent form we might consider for the BAO correlation function is the superposition of a Gaussian and a featureless (e.g., polynomial) fitting function. Such empirical models have been considered in e.g., [45–47]. For a universe with statistical homogeneity and isotropy, we expect the BAO characteristic scale to be statistically independent of the direction of separation of the galaxies relative to our position, up to observational biases such as redshift-space distortions and non-representative sampling of the underlying galaxy distribution. These considerations motivate the following empirical model as a function of the Lagrangian separation D and radial fraction μ :

$$\xi_{Fit}(D^{\text{tr}}, \mu^{\text{tr}}) = (D^{\text{tr}})^2 A \exp \left[\frac{-(D^{\text{tr}} - r_{\text{BAO}})^2}{2\sigma^2} \right] + C_0(\mu^{\text{tr}}) + \frac{C_1(\mu^{\text{tr}})}{D^{\text{tr}}} + \frac{C_2(\mu^{\text{tr}})}{(D^{\text{tr}})^2} \quad (4.1)$$

where the superscript “tr” refers to the underlying “true” cosmology. The polynomial terms model the underlying featureless shape of the correlation function without the BAO feature and are equivalent in form to those of [24]. The scaled Gaussian empirically models the BAO feature, and replaces the Λ CDM power spectrum model of [24].

We note that the local maximum of the 2-point correlation function at the BAO peak does not in general correspond to the BAO scale in a particular cosmological model (for example, these two characteristic scales differ by $\sim 2 - 3\%$ in Λ CDM cosmology, a systematic difference which is significantly larger than the statistical measurement error in the scale). This is a significant issue for empirical modelling, if we wish to incorporate predictions of the underlying BAO scale.

To partially address this issue, we include a factor $(D^{\text{tr}})^2$ multiplying the Gaussian term in eq. (4.1), which changes the position of the local maximum in order to produce a closer match to the expected fiducial characteristic scale r_{BAO} of the Λ CDM mock catalogues, within the current level of statistical precision. This calibration would need to be re-assessed in the context of other cosmological models.¹¹ Furthermore, we do not assume any calibration of r_{BAO} in this study, instead quoting results for r_{BAO}/α , and focus our investigation on the significance of the BAO feature and the self-consistency of the radial and transverse wedges.

We allow for μ^{tr} dependence in the polynomial terms of the fitting function (4.1) since observational biases such as redshift-space distortions can depend on the separation of the galaxies relative to the line of sight. We assume that the BAO feature is independent of μ^{tr} , although asymmetric biases might enter here as well. However, from our mock investigations (see section 4.2) we find that we successfully recover the BAO scale and the distortion parameter ϵ with the fitting function (4.1), justifying this form at least for the Λ CDM model.

We can approximate eq. (4.1) in terms of the model cosmology through the Alcock-Paczyński scaling explained in section 2.3. Substituting D^{tr} with the approximation (2.16) and μ^{tr} with the approximation (2.17), the empirical model (4.1) can be written

$$\begin{aligned} \xi_{Fit}(D^{\text{tr}}, \mu^{\text{tr}}) &\approx \xi_{Fit}\left(\tilde{D}^{\text{tr}}(D, \mu; \alpha_{\parallel}, \alpha_{\perp}), \tilde{\mu}^{\text{tr}}(D, \mu; \alpha_{\parallel}, \alpha_{\perp})\right) \\ &= (D)^2 \alpha_{\perp}^2 (1 + \psi \mu^2) A e^{-\left(D \alpha_{\perp} \sqrt{1 + \psi \mu^2} - r_{\text{BAO}}\right)^2 / (2\sigma^2)} + C_0(\mu) + \frac{C_1(\mu)}{D} + \frac{C_2(\mu)}{(D)^2}, \end{aligned} \quad (4.2)$$

with

$$\psi \equiv \left(\frac{\alpha_{\parallel}}{\alpha_{\perp}}\right)^2 - 1 = (1 + \epsilon)^6 - 1, \quad (4.3)$$

and where $\tilde{D}^{\text{tr}}(D, \mu; \alpha_{\parallel}, \alpha_{\perp})$ is the approximation of D^{tr} given by (2.16) and $\tilde{\mu}^{\text{tr}}(D, \mu; \alpha_{\parallel}, \alpha_{\perp})$ is the approximation of μ^{tr} given by (2.17). Thus, when $\xi_{Fit}(D^{\text{tr}}, \mu^{\text{tr}})$ is expressed in terms of D and μ through the approximation of the Alcock-Paczyński scaling, it has the form of a Gaussian in D scaled by D^2 plus first and second order polynomial terms in D^{-1} . The coefficients of the Gaussian in the basis of the model cosmology eq. (4.2) are now dependent on μ .

As discussed in section 2.5, we construct two wedge correlation functions and the angle-averaged correlation function, by averaging eq. (4.2) over μ -ranges. For current galaxy surveys, it is in practice not useful to consider finer binning in μ , as the noise in the 2-point

¹¹Models that are not developed with respect to perturbation theory cannot be tested against the full information in the CMB anisotropies, and are consequently more weakly constrained than Λ CDM scenarios.

correlation function increases with decreasing bin-size, and two wedges already capture the information on α and ϵ .

In the regime of $\psi D/\sigma \ll 1$, we may expand the Gaussian part of the fitting function (4.2) to linear order in $\psi D/\sigma$ before performing the averaging in μ . This has the advantage of providing an analytic expression for the average. Expanding the Gaussian part of $\xi_{Fit,\mathcal{N}}$ (4.2) to linear order in $\psi D/\sigma$ we have

$$\begin{aligned}\xi_{Fit,\mathcal{N}}(D, \mu) &\approx (D)^2 \alpha_{\perp}^2 (1 + \psi \mu^2) A e^{-(D\alpha_{\perp} - r_{BAO})^2/(2\sigma^2) - \psi \mu^2 D\alpha_{\perp} (D\alpha_{\perp} - r_{BAO})/(2\sigma^2)} \\ &\approx (D)^2 \alpha_{\perp}^2 A e^{-(D\alpha_{\perp} - r_{BAO})^2/(2\sigma^2)} \left(1 - \frac{\psi \mu^2 D\alpha_{\perp} (D\alpha_{\perp} - r_{BAO})}{2\sigma^2} + \psi \mu^2 \right),\end{aligned}\quad (4.4)$$

and taking the average in μ over the range $[\mu_1, \mu_2]$ we have

$$\begin{aligned}&\frac{1}{\mu_2 - \mu_1} \int_{\mu_1}^{\mu_2} d\mu \xi_{Fit,\mathcal{N}}(D, \mu) \\ &\approx (D)^2 \alpha_{\perp}^2 A e^{-(D\alpha_{\perp} - r_{BAO})^2/(2\sigma^2)} \left[1 + \frac{1}{3} \psi \frac{\mu_2^3 - \mu_1^3}{\mu_2 - \mu_1} \left(1 - \frac{D\alpha_{\perp} (D\alpha_{\perp} - r_{BAO})}{2\sigma^2} \right) \right] \\ &\approx (D)^2 \alpha_{\perp}^2 (1 + \kappa) A e^{-[D\alpha_{\perp} (1 + \frac{1}{2}\kappa) - r_{BAO}]^2/(2\sigma^2)} \\ &\approx (D)^2 \tilde{A} e^{-(D - \tilde{r}_{BAO})^2/(2\tilde{\sigma}^2)},\end{aligned}\quad (4.5)$$

where

$$\kappa \equiv \frac{1}{3} \psi \frac{\mu_2^3 - \mu_1^3}{\mu_2 - \mu_1}, \quad (4.6)$$

we have neglected terms $\mathcal{O}(\kappa^2)$ at each step, and in the final line the distorted Gaussian parameters are defined by

$$\tilde{r}_{BAO} \equiv \frac{1 - \frac{1}{2}\kappa}{\alpha_{\perp}} r_{BAO}, \quad \tilde{\sigma} \equiv \frac{1 - \frac{1}{2}\kappa}{\alpha_{\perp}} \sigma, \quad \tilde{A} \equiv \alpha_{\perp}^2 (1 + \kappa) A. \quad (4.7)$$

The final wedge fitting function thus yields

$$\xi_{Fit, [\mu_1, \mu_2]}(D) = (D)^2 \tilde{A} e^{-(D - \tilde{r}_{BAO})^2/(2\tilde{\sigma}^2)} + \bar{C}_0 + \frac{\bar{C}_1}{D} + \frac{\bar{C}_2}{(D)^2}, \quad (4.8)$$

where \bar{C}_0 , \bar{C}_1 , and \bar{C}_2 are unspecified coefficients depending on the interval $[\mu_1, \mu_2]$. In the following, we investigate some limits of the wedge fitting function eq. (4.8).

We emphasise that the applicability of the expansion in eq. (4.4) and the resulting expression for the wedge fitting function (4.8) must be checked for a given application. When $\psi D/\sigma \ll 1$ is not satisfied over the fitting range in D , one must average the full expression (4.2) over μ in order to obtain the exact expression for the empirical wedge fitting function. We use the approximation (4.8) in our analysis, and confirm its validity by repeating our analysis using the exact expression. (See section 5.2 for a discussion of this point.)

The ideal wedge limit. Let us consider the ideal wedge limit $\mu_2 \rightarrow \mu_1$, in which the bin width is reduced to zero. In this limit we have

$$\kappa = \psi \mu_1^2 = \psi \mu_2^2. \quad (4.9)$$

Working to linear order in the anisotropic distortion parameter, so that by (4.3) $\alpha_{\parallel}/\alpha_{\perp} \simeq 1 + 3\epsilon$, the distorted Gaussian parameters (4.7) in this case read

$$\tilde{r}_{BAO} = \frac{r_{BAO}}{\alpha_{\perp}^{1-\mu_1^2} \alpha_{\parallel}^{\mu_1^2}}, \quad \tilde{\sigma} \equiv \frac{\sigma}{\alpha_{\perp}^{1-\mu_1^2} \alpha_{\parallel}^{\mu_1^2}}, \quad \tilde{A} \equiv \alpha_{\perp}^{2-2\mu_1^2} \alpha_{\parallel}^{2\mu_1^2} A, \quad (4.10)$$

e.g., for the pure transverse wedge ($\mu_1^2 = \mu_2^2 = 0$) and pure radial wedge ($\mu_1^2 = \mu_2^2 = 1$), one can check that this expression reduces to the expected scaling by α_{\perp} and α_{\parallel} respectively. For $\mu_1^2 = \mu_2^2 = \frac{1}{2}$, eq. (4.10) is symmetric in α_{\perp} and α_{\parallel} , as expected.

The observational wedges. In practice we need to make a crude binning in μ in order to increase the galaxy counts for each bin. Thus in the further analysis we shall work with two μ -bins and denote $\mu_1 = 0, \mu_2 = \frac{1}{2}$ the transverse wedge, and $\mu_1 = \frac{1}{2}, \mu_2 = 1$ the radial wedge. For the transverse and radial wedges we find respectively for κ

$$\kappa_{\perp} = \frac{1}{12}\psi, \quad \kappa_{\parallel} = \frac{7}{12}\psi, \quad (4.11)$$

which on substitution in eq. (4.7), to linear order in ϵ , yield the distorted Gaussian parameters

$$\tilde{r}_{BAO\perp} = \frac{r_{BAO}}{\alpha_{\perp}^{11/12} \alpha_{\parallel}^{1/12}}, \quad \tilde{\sigma}_{\perp} \equiv \frac{\sigma}{\alpha_{\perp}^{11/12} \alpha_{\parallel}^{1/12}}, \quad \tilde{A}_{\perp} \equiv \alpha_{\perp}^{11/6} \alpha_{\parallel}^{1/6} A, \quad (4.12)$$

and

$$\tilde{r}_{BAO\parallel} = \frac{r_{BAO}}{\alpha_{\perp}^{5/12} \alpha_{\parallel}^{7/12}}, \quad \tilde{\sigma}_{\parallel} \equiv \frac{\sigma}{\alpha_{\perp}^{5/12} \alpha_{\parallel}^{7/12}}, \quad \tilde{A}_{\parallel} \equiv \alpha_{\perp}^{5/6} \alpha_{\parallel}^{7/6} A, \quad (4.13)$$

for the transverse and radial wedges, respectively. Note that eq. (4.12) and (4.13) are not symmetric under interchange $\alpha_{\perp} \leftrightarrow \alpha_{\parallel}$. This asymmetry between the radial and transverse wedges comes from the fact that we have defined the wedge as an unweighted average in μ .

The isotropic wedge. For the isotropic wedge ($\mu_1 = 0, \mu_2 = 1$) we have $\kappa = \psi/3$ which to linear order in ϵ leads to the ‘‘isotropically distorted’’ Gaussian parameters

$$\tilde{r}_{BAO} = \frac{r_{BAO}}{\alpha}, \quad \tilde{\sigma} \equiv \frac{\sigma}{\alpha}, \quad \tilde{A} \equiv \alpha^2 A. \quad (4.14)$$

Note that only the isotropic scaling parameter α enters here, and not the anisotropic distortion parameter ϵ .

4.2 Testing on Λ CDM mocks

We now apply the fitting function (4.8) to Λ CDM mocks, to test if we recover the fiducial BAO scale and distortion parameter. To do this we perform fits to the mean correlation function of the QPM mocks based on the CMASS NGC and LOWZ NGC galaxy distributions, assuming a fiducial flat Λ CDM model with $\Omega_{M0} = 0.3$. First we perform a fit to the isotropic correlation function $\xi(D)$ with the fitting function discussed in section 4.1. Next we perform a joint fit to estimates of the radial wedge $\xi_{\parallel}(D)$ and transverse wedge $\xi_{\perp}(D)$ functions. We fit to correlation function measurements in the range $D \in [50; 150]$ Mpc/ h with a bin size of 5 Mpc/ h .

For the likelihood function \mathcal{L} of the data given the model, we assume a Gaussian distribution with mean ξ_{Fit}

$$\mathcal{L}\left(\hat{\xi} \mid \xi_{\text{Fit}}\right) \propto \exp(-\chi^2/2), \quad (4.15)$$

with

$$\chi^2 = Z^T \underline{\underline{C}}_{\hat{\xi}}^{-1} Z, \quad Z = \hat{\xi} - \xi_{\text{Fit}}, \quad (4.16)$$

where $\hat{\xi}$ is the binned estimate of the (isotropic or wedge) 2-point correlation function, and $\bar{\xi}$ is its average over the mocks. For the wedge analysis, the transverse and radial estimates are combined into a single vector $\hat{\xi}$ in order to perform a combined fit, taking into account the covariance between the wedges. ξ_{Fit} is the fitting function prescribed in eq. (4.8). The covariance matrix of $\hat{\xi}$ is given by the covariance of the individual measurements $\hat{\xi}$ scaled by the number of mocks over which we take the mean, N_{mean}

$$\underline{\underline{C}}_{\bar{\xi}} = \frac{1}{N_{\text{mean}}} \underline{\underline{C}}_{\hat{\xi}}, \quad \underline{\underline{C}}_{\hat{\xi}} = \overline{(\hat{\xi} - \bar{\xi})(\hat{\xi} - \bar{\xi})^T}, \quad (4.17)$$

where the overbar represents the averages over the number of mocks, N_{mocks} . In this analysis we have $N_{\text{mocks}} = 1000$ for both CMASS and LOWZ. N_{mean} is chosen such that $\chi^2/N_{\text{dof}} \sim 1$ in order to not to go beyond the regime of applicability of the empirical fitting function ($N_{\text{mean}} = 40$ for CMASS and $N_{\text{mean}} = 80$ for LOWZ), where N_{dof} is the number of independent degrees of freedom.

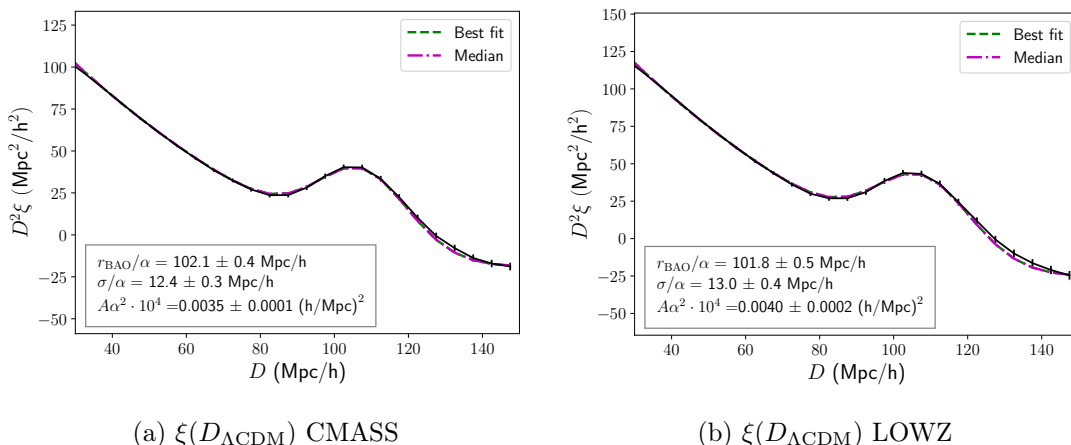


Figure 3: Fit to the isotropic wedge $\xi(D_{\Lambda\text{CDM}})$ of the mean of the CMASS NGC and LOWZ NGC QPM mocks respectively. $D_{\Lambda\text{CDM}}$ is the Lagrangian distance evaluated at present times for ΛCDM with $\Omega_{M0} = 0.3$. The model fit includes 6 parameters (r_{BAO}/α , σ/α , $A\alpha^2$, C_0 , C_1 , C_2). The best fit (green line) is the fit that maximises the likelihood function. The median fit (purple line) is based on the 50% quantiles of the Bayesian posterior, resulting from conservative priors (meaning priors that span the significant volume of the likelihood). Mean values of r_{BAO}/α , σ/α , and $A\alpha^2$ with 1σ equal tail credible intervals are superimposed on the plots.

We determine the parameters of ξ_{Fit} in both a frequentist and Bayesian setting: that is, we find frequentist best fit parameters as well as Bayesian median parameters with conservative priors. The results of the fit to the isotropic correlation function for the CMASS

and LOWZ QPM mock mean are shown in figure 3, and the results of the fit to the wedges are shown in figure 4. The estimates of the parameters describing the isotropic BAO feature ($\frac{r_{\text{BAO}}}{\alpha}$, $\frac{\sigma}{\alpha}$, $A\alpha^2$) are in good agreement between the isotropic and wedge analyses. The results for the estimated isotropic BAO scale are $\frac{r_{\text{BAO}}}{\alpha} = 102.1 \pm 0.4 \text{ Mpc}/h$ for CMASS and $\frac{r_{\text{BAO}}}{\alpha} = 101.8 \pm 0.5 \text{ Mpc}/h$ for LOWZ, and the results for the estimated anisotropic distortion parameter are $\epsilon = 0.0005 \pm 0.0035$ for CMASS and $\epsilon = 0.0008 \pm 0.0043$ for LOWZ.

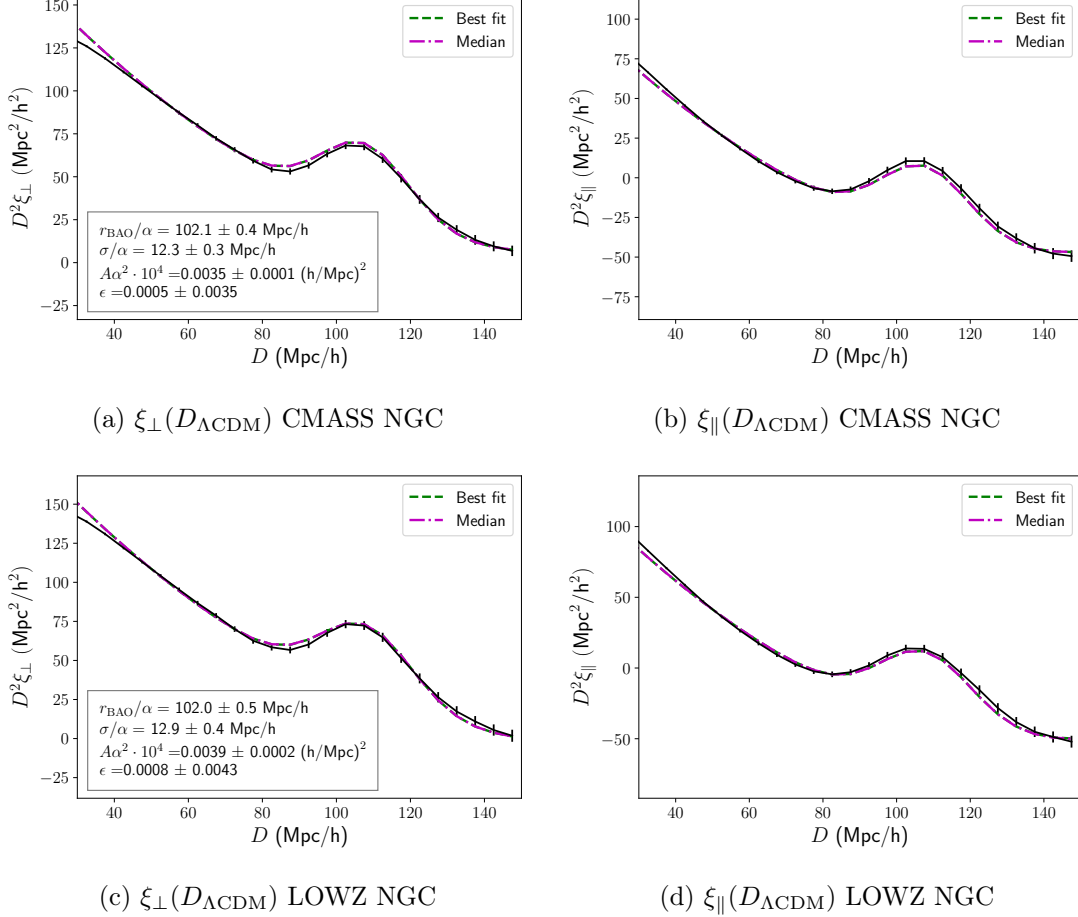


Figure 4: Combined fit to the transverse wedge $\xi_{\perp}(D_{\Lambda\text{CDM}})$ and radial wedge $\xi_{\parallel}(D_{\Lambda\text{CDM}})$ of the mean of the CMASS NGC and LOWZ NGC QPM mocks respectively, where $D_{\Lambda\text{CDM}}$ is the Lagrangian distance evaluated at present times for ΛCDM with $\Omega_{M0} = 0.3$. The model fit includes 10 parameters ($\frac{r_{\text{BAO}}}{\alpha}$, $\frac{\sigma}{\alpha}$, $A\alpha^2$, ϵ , $\bar{C}_{0\perp}$, $\bar{C}_{1\perp}$, $\bar{C}_{2\perp}$, $\bar{C}_{0\parallel}$, $\bar{C}_{1\parallel}$, $\bar{C}_{2\parallel}$). The best fit (green line) is the fit that maximises the likelihood function. The median fit (purple line) is based on the 50% quantiles of the Bayesian posterior, resulting from conservative priors (meaning priors that span the significant volume of the likelihood). The numerical values superimposed on the plot of ξ_{\perp} are the mean values with 1σ equal tail credible intervals.

As noted in section 3.3, the acoustic scale of the model underlying the QPM mocks is $r_s = 103.05 \text{ Mpc}/h$. Since the QPM mocks are generated using $\Omega_{M0} = 0.29$, and our fiducial model has $\Omega_{M0} = 0.30$, we have $\alpha(\bar{z} = 0.55) = 1.005$, and $\alpha(\bar{z} = 0.32) = 1.003$. We thus

compute expected fiducial values

$$\frac{r_s}{\alpha(\bar{z} = 0.55)} = 102.5 \text{ Mpc}/h, \quad \frac{r_s}{\alpha(\bar{z} = 0.32)} = 102.7 \text{ Mpc}/h \quad (4.18)$$

$$\epsilon(\bar{z} = 0.55) = 0.0013, \quad \epsilon(\bar{z} = 0.32) = 0.0008 \quad (4.19)$$

As seen in the isotropic results in figure 3, the BAO scale is recovered to a precision of $0.4\% \pm 0.4\%$ for CMASS and $0.9\% \pm 0.5\%$ for LOWZ. The difference between the measured and the model ϵ -parameter is $|\Delta\epsilon| \lesssim 0.0008$, which is much smaller than typical errors in ϵ in the context of Λ CDM template-fitting approaches to BAO.

We note that $\sim 1\%$ systematic error is significant in standard BAO template-fitting approaches, where the statistical errors in the BAO scale measurement from the latest galaxy redshift surveys are around 1%, and the contribution from systematic errors in a Λ CDM model universe are significantly less than 1% [48]. Systematic errors in an empirical fitting procedure will inevitably be larger, and dependent on the cosmological model.¹² However, the errors in the underlying calibration of the BAO scale from the CMB are also larger in models with greater uncertainties in the underlying physical parameters. In this paper, we will mainly be interested in the ϵ parameter as a consistency check of the tested fiducial cosmologies, and in comparing the significance of the BAO feature between the tested models, and do not include a calibration of the underlying BAO scale.

We experimented with modifications of eq. (4.8), allowing for a relative scaling of the wedge amplitudes, wedge widths, or both. The resulting fits were of similar quality to that of eq. (4.8) from an Akaike Information Criterion perspective. Thus we had no Λ CDM-based motivation for introducing additional parameters in the analysis of the galaxy survey. We note, however, that for models with more complicated curvature evolution than Λ CDM, there might be physical effects equivalent to the Λ CDM redshift-space distortions but possibly with stronger magnitude, distorting the relative amplitude and width of the BAO feature in the two wedges.¹³

We also experimented with different scaling behaviour of the Lagrangian distance D^{tr} in eq. (4.1) – for example, changing the scaling $(D^{\text{tr}})^2$ of the Gaussian function to $(D^{\text{tr}})^n$ with different values of n . The inferred peak of the Gaussian changed as expected, in some cases being significantly different from the BAO scale. However, ϵ was consistent with the expected values in eq. (4.19) for all investigated modifications of the fitting function.

5 Data analysis

The empirical procedure developed in this paper can be applied to a wide class of cosmological models. In this analysis, we consider two fiducial model frameworks – the timescape model

¹²A fiducial Λ CDM fitting function per construction gives back the correct BAO scale when fitted to mocks generated from that same fiducial Λ CDM model. Any empirical fitting model, aiming at analysing BAO features for a broader class of models will yield larger systematics in the context of Λ CDM model simulations than the fitting procedure adapted specifically to Λ CDM. The price to pay for introducing a flexible fitting function adaptable to a large range of cosmologies, is exactly that it is not adapted to a particular cosmology.

¹³There is no obvious reason for this to be the case in the timescape model, however, since it implements a “uniform quasilocal Hubble flow condition” [17, 23]. Calculations of the amplitude of redshift-space distortions require the development of a framework analogous to standard cosmological perturbation theory, which is yet to be done for the timescape cosmology. Estimates of the amplitude of non-kinematic differential expansion [49] have been made using the Lemaitre-Tolman-Bondi models for local structures on scales of order 10–60 Mpc [50], with the result that differences from the standard model expectation are smaller than current measurement uncertainties in peculiar velocities. Thus we would not expect substantial differences from the amplitude of the standard Kaiser effect [51], at least within this class of models.

and the spatially flat Λ CDM model, with $\Omega_{M0} = 0.3$ in both cases. We note that both the Λ CDM and timescape models have a spherically symmetric effective adapted geometry with a large curvature scale proportional to the Hubble distance $\sim c/H_0$, which is in both models of order 3 Gpc/ h . Thus the curvature scale is of order the survey diameter. The Lagrangian distance introduced in section 2.1 between two galaxies separated around ~ 100 Mpc/ h is thus well approximated by eq. (2.7) with correction terms¹⁴ of order $\lesssim 10^{-3}$. We caution that our results may not be suitable for extrapolation to other model cosmologies, depending on the Alcock-Paczyński scaling.

We estimate the 2-point correlation function in each fiducial model for the CMASS and LOWZ NGC and SGC regions using the LS estimator described in section 2.5. We compute the isotropic correlation function estimator $\hat{\xi}(D)$, along with the radial and transverse wedge correlation function estimators, $\hat{\xi}_{\parallel}(D)$ and $\hat{\xi}_{\perp}(D)$, defined in eq. (2.32). We use the covariance matrix $\underline{\underline{C}}_{\xi}$ formulated in eq. (4.17), computed from the QPM mocks described in section 3.3, to estimate the variance of the correlation function over realisations of an imagined ensemble of galaxy catalogues, of which our galaxy catalogue is a single realisation. We expect different models to Λ CDM, with different models for structure formation and global geometry, to give rise to a different random process underlying our measured galaxy catalogue. However, we shall assume that the Λ CDM estimate provides a reasonable lowest-order approximation of the covariance.

We combine the estimated correlation functions for the NGC and SGC regions using the inverse covariance weighting [7, 52]

$$\hat{\xi}_{\text{comb}} = \underline{\underline{C}}_{\text{comb}}^{-1} \left(\underline{\underline{C}}_{\text{NGC}}^{-1} \hat{\xi}_{\text{NGC}} + \underline{\underline{C}}_{\text{SGC}}^{-1} \hat{\xi}_{\text{SGC}} \right), \quad (5.1)$$

where

$$\underline{\underline{C}}_{\text{comb}}^{-1} = \underline{\underline{C}}_{\text{NGC}}^{-1} + \underline{\underline{C}}_{\text{SGC}}^{-1}, \quad (5.2)$$

is the inverse covariance of the combined measurement, and where ξ represents either the isotropic correlation functions $\xi(D)$ or the combined wedge correlation function $(\xi_{\parallel}(D), \xi_{\perp}(D))$. We experimented with different methods of combining the NGC and SGC measurements, and found that our results were robust to the exact weighting scheme used.

5.1 Isotropic fitting analysis

The estimated isotropic correlation function and best fit and median models are displayed in figure 5 for Λ CDM and in figure 6 for the timescape cosmology, and the results of the fits are summarised in table 1. The Gaussian peak component is significant in the CMASS isotropic correlation function at the 4.6σ level for Λ CDM and at the 3.8σ level for timescape. We quantify the significance of the peak as the posterior probability of having $\alpha^2 A > 0$.¹⁵ For the LOWZ correlation function, the peak is significant at the 2.4σ level for Λ CDM and at the 1.9σ level for timescape.

We have used conservative priors for our fits to both timescape and Λ CDM, meaning (log-)uniform priors that span all regions of parameter space of significant likelihood volume. For the sake of comparing our Λ CDM results with the standard fiducial Λ CDM analysis of

¹⁴See appendix A for an explicit derivation of the correction terms.

¹⁵We note that this is different to the typical way of quantifying BAO significance in Λ CDM-based fitting, where a reference power spectrum with no BAO feature is used to assess the increase of quality in fit when introducing the BAO feature [53].

[24] and [25], we have repeated the fit with narrow Gaussian error bars on $\sigma_{\text{BAO}}/\alpha$ with mean and standard deviation as determined by the isotropic mock fit of section 4.2. For both models, using this prior increases the significance of the BAO feature and decreases the errors in r_{BAO}/α . We only compare model fits when the priors are equally restrictive for both models and, unless otherwise stated, we comment on the analysis with conservative priors.

The results for r_{BAO}/α and $\sigma_{\text{BAO}}/\alpha$ are consistent between the LOWZ and CMASS samples for both timescape and Λ CDM. The results for the CMASS BAO peak positions for the conservative prior analysis are $r_{\text{BAO}}/\alpha = 102.0 \pm 1.7$ Mpc/ h for Λ CDM and 95.4 ± 1.8 Mpc/ h for timescape. The equivalent results for LOWZ are 99.9 ± 4.3 Mpc/ h for Λ CDM and 93.4 ± 4.9 Mpc/ h for timescape. The sign and magnitude of the relative peak positions of timescape and Λ CDM are consistent with figure 1 within the statistical error bars of the analysis. This can be realised by computing the relative isotropic AP-scaling α (2.14) between Λ CDM and timescape based on figure 1 and comparing it to the ratio of the measured peak positions r_{BAO}/α of the models.

Values of the Hubble constant for the timescape model obtained from CMB constraints can be up to 10% smaller than for the Λ CDM model [33]. Thus for typical values of H_0 the estimated isotropic peak position in units Mpc may in fact be slightly *larger* for timescape than the analogous peak position for Λ CDM.

The fits are reasonably good, all with a minimum χ^2 value of reasonable probability. The most extreme value is $\chi^2 = 22$ for the timescape LOWZ fit, the probability of $\chi^2 > 22$ being 8% for 14 degrees of freedom.

When we include a prior in σ , our Λ CDM results for the isotropic peak position r_{BAO}/α are in $\lesssim 1\%$ agreement with those found in the fiducial Λ CDM analysis considered in e.g., [24] and [25]. The magnitude of the error bars are also comparable to those found in standard analyses. As an example, we compare our results with the isotropic pre-reconstruction DR12 results of table 8 in [25], derived assuming the fiducial cosmology $\Omega_{M0,\text{fid}} = 0.29$ and $r_{\text{BAO},\text{fid}} = 103.0$ Mpc/ h . The isotropic CMASS measurement yields $\tilde{\alpha} = \alpha(\Omega_{M0} = 0.29) \frac{r_{\text{BAO},\text{fid}}}{r_{\text{BAO}}} = 1.015 \pm 0.013$, which together with the value of $r_{\text{BAO},\text{fid}}$ yields $\frac{r_{\text{BAO}}}{\alpha(\Omega_{M0}=0.29)} = 101.4 \pm 1.3$ Mpc/ h , and finally scaling the result with the α -ratio of Λ CDM fiducial $\Omega_{M0,\text{fid}} = 0.29$ and $\Omega_{M0} = 0.3$ we have $\frac{r_{\text{BAO}}}{\alpha(\Omega_{M0}=0.30)} = 100.9 \pm 1.3$ Mpc/ h . This result is within 1σ agreement with the Λ CDM results in table 1 for both the conservative prior analysis and for the analysis with a narrow Gaussian prior in $\sigma_{\text{BAO}}/\alpha$. The analogous isotropic LOWZ result from table 8 in [25] reads $\tilde{\alpha} = \alpha(\Omega_{M0} = 0.29) \frac{r_{\text{BAO},\text{fid}}}{r_{\text{BAO}}} = 1.009 \pm 0.030$, which gives $\frac{r_{\text{BAO}}}{\alpha(\Omega_{M0}=0.30)} = 101.7 \pm 3.1$ Mpc/ h , in agreement with the Λ CDM results in table 1 for the conservative prior analysis and for the narrow Gaussian prior in $\sigma_{\text{BAO}}/\alpha$.

5.2 Anisotropic fitting analysis

We now turn to the wedge analysis, which is useful for examining the consistency of the BAO feature in the transverse and radial separation of galaxy pairs. The results of fitting the empirical parameters describing the BAO feature are shown in table 2. The measurements of the anisotropic distortion parameter in CMASS are $\epsilon = -0.021 \pm 0.017$ for Λ CDM and $\epsilon = 0.021 \pm 0.017$ for timescape, and the LOWZ results are $\epsilon = -0.022 \pm 0.084$ for Λ CDM and $\epsilon = 0.013 \pm 0.110$ for timescape. The CMASS and LOWZ results for the peak position r_{BAO}/α and the width $\sigma_{\text{BAO}}/\alpha$ are consistent within 1σ for both Λ CDM and the timescape model.

The Gaussian peak in the CMASS wedge correlation functions has a significance of $\sim 4.8\sigma$ for Λ CDM and $\sim 3.9\sigma$ for timescape. For LOWZ, the peak has a significance of

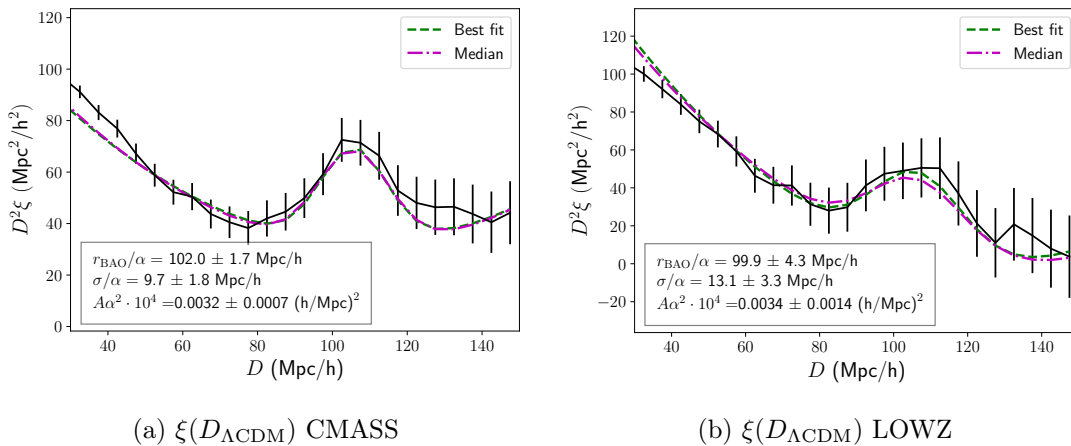


Figure 5: Fit to the isotropic wedge $\xi(D_{\Lambda\text{CDM}})$ of the CMASS and LOWZ survey respectively, where $D_{\Lambda\text{CDM}}$ is the Lagrangian distance evaluated at present times for ΛCDM with $\Omega_{M0} = 0.3$. The model fit includes 6 parameters ($\frac{r_{\text{BAO}}}{\alpha}$, $\frac{\sigma}{\alpha}$, $A\alpha^2$, C_0 , C_1 , C_2). The best fit (green line) is the fit that maximises the likelihood function. The median fit (purple line) is based on the 50% quantiles of the Bayesian posterior, resulting from conservative priors (meaning priors that span the significant volume of the likelihood). Mean values of $\frac{r_{\text{BAO}}}{\alpha}$, $\frac{\sigma}{\alpha}$, and $A\alpha^2$ with 1σ equal tail credible intervals are superimposed on the plots.

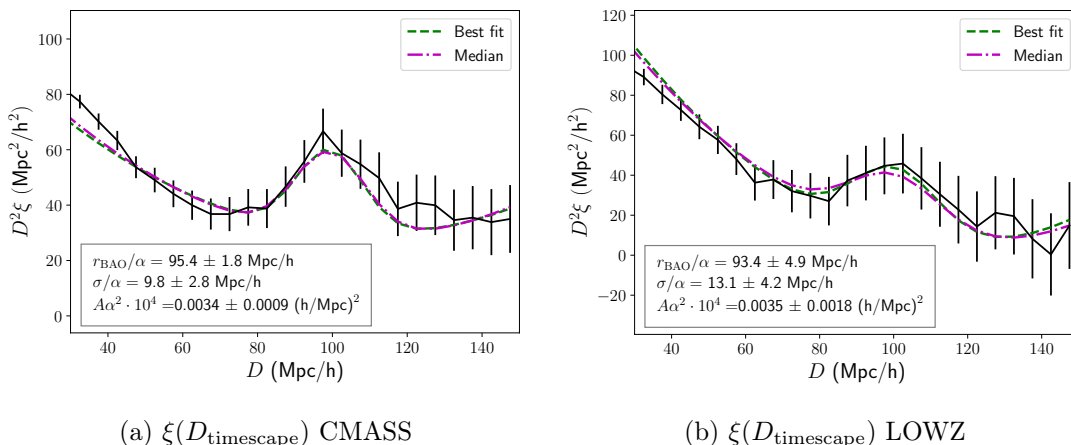


Figure 6: Fit to the isotropic wedge $\xi(D_{\text{timescape}})$ of the CMASS and LOWZ survey respectively, where $D_{\text{timescape}}$ is the Lagrangian distance evaluated at present times for the timescape model with $\Omega_{M0} = 0.3$. The model fit includes 6 parameters ($\frac{r_{\text{BAO}}}{\alpha}$, $\frac{\sigma}{\alpha}$, $A\alpha^2$, C_0 , C_1 , C_2). The best fit (green line) is the fit that maximises the likelihood function. The median fit (purple line) is based on the 50% quantiles of the Bayesian posterior, resulting from conservative priors (meaning priors that span the significant volume of the likelihood). Mean values of $\frac{r_{\text{BAO}}}{\alpha}$, $\frac{\sigma}{\alpha}$, and $A\alpha^2$ with 1σ equal tail credible intervals are superimposed on the plots.

$\sim 1.4\sigma$ and $\sim 1.3\sigma$ for ΛCDM and timescape respectively. As above, the significance of the peak is quantified as the posterior probability of having $\alpha^2 A > 0$.

We note that the values of epsilon gives $\psi \approx 0.1$, for which the expansion in eq. (4.4)

Isotropic fit ξ	$\alpha^2 A \cdot 10^4$	r_{BAO}/α	$\sigma_{\text{BAO}}/\alpha$	χ^2/N_{dof}
$\Lambda\text{CDM CMASS}$	0.0032 ± 0.0007	102.0 ± 1.7	9.7 ± 1.8	17/14
$\Lambda\text{CDM LOWZ}$	0.0034 ± 0.0014	99.9 ± 4.3	13.1 ± 3.3	19/14
Timescape CMASS	0.0034 ± 0.0009	95.4 ± 1.8	9.8 ± 2.8	21/14
Timescape LOWZ	0.0035 ± 0.0018	93.4 ± 4.9	13.1 ± 4.2	22/14
$\Lambda\text{CDM CMASS } \mathcal{N}_{\sigma_{\text{BAO}}/\alpha}$	0.0037 ± 0.0007	100.4 ± 1.5	12.2 ± 0.3	17/14
$\Lambda\text{CDM LOWZ } \mathcal{N}_{\sigma_{\text{BAO}}/\alpha}$	0.0035 ± 0.0011	100.6 ± 3.0	12.2 ± 0.3	19/14

Table 1: Results of fitting the isotropic correlation function of CMASS and LOWZ. The parameter estimates shown are the Bayesian median with 1σ equal tail credible intervals. Conservative priors (meaning priors that span the significant volume of the likelihood) are used for all parameters in all fits, except for the ΛCDM fits labelled $\mathcal{N}_{\sigma_{\text{BAO}}/\alpha}$, which use a narrow Gaussian prior with mean and width as determined in the mock analysis of section 4.2. The minimum χ^2 value divided by number of degrees of freedom N_{dof} is also quoted. r_{BAO}/α and $\sigma_{\text{BAO}}/\alpha$ are in units of Mpc/h . A is in units of $(\text{Mpc}/h)^2$.

is not guaranteed to hold for the fitting range $D \in [50; 150] \text{ Mpc}/h$. We checked the validity of the approximate fitting model eq. (4.8) by comparing to the exact wedge fitting functions calculated from the average of eq. (4.2) over μ , and found that best fit parameter results derived in our linearised analysis receive corrections of order $\sim 10\%$ of the error bars on the same parameters. Since the corrections are an order of magnitude smaller than the error bars, we ignore these corrections here and quote the results from the linearised analysis.

The best fit and median models of eq. (4.8) are shown superimposed on the ξ_{\perp} and ξ_{\parallel} measurements for the spatially flat ΛCDM fiducial cosmology in figure 7 and for the timescape fiducial cosmology in figure 8. The most extreme χ^2 value is for the timescape CMASS fit with $\chi^2 = 49$, with 2% probability of $\chi^2 > 49$ for 30 degrees of freedom.

The significance and precision of the acoustic peak in the LOWZ sample is significantly increased by imposing a prior in $\sigma_{\text{BAO}}/\alpha$, which is illustrated for the ΛCDM case in table 2. Using narrow Gaussian priors with mean and width determined by the mock analysis of section 4.2, the significance of the peak goes up to 2σ and the errors in r_{BAO}/α decrease by $\sim 30\%$. The measurements of $\alpha^2 A$, r_{BAO}/α , and $\sigma_{\text{BAO}}/\alpha$ for the wedge analysis are in good agreement with those of the isotropic analysis in table 1 for both timescape and ΛCDM . We note that the errors on $\alpha^2 A$, r_{BAO}/α , and $\sigma_{\text{BAO}}/\alpha$ all decrease when going from the isotropic analysis to the anisotropic analysis for CMASS, whereas they all increase for LOWZ. This might be because of the strong correlation between $\sigma_{\text{BAO}}/\alpha$ and the remaining parameters of the analysis: a posterior which widens in σ/α is likely to widen in the other parameters as well.

The results of our fiducial ΛCDM analysis displayed in table 2 are in good agreement with previous measurements reported by [24] and [25]. For example, table 8 of [25] reports $\epsilon = -0.016 \pm 0.020$ for a DR12 CMASS pre-reconstruction wedge analysis which, when transformed through AP-scaling eq. (2.14) from the fiducial model $\Omega_{M0} = 0.29$ of [25] to the fiducial model $\Omega_{M0} = 0.3$ of this paper, produces $\epsilon = -0.015 \pm 0.020$. This is in agreement well within 1σ of our results listed in table 2. The analogous result for the LOWZ sample in table 8 of [25] is 0.026 ± 0.041 , which AP-scaled gives $\epsilon = 0.025 \pm 0.041$, which is in agreement with our ΛCDM results for LOWZ in table 2 at the 1σ level.

The anisotropic distortion parameter ϵ describes how the fiducial model is distorted in

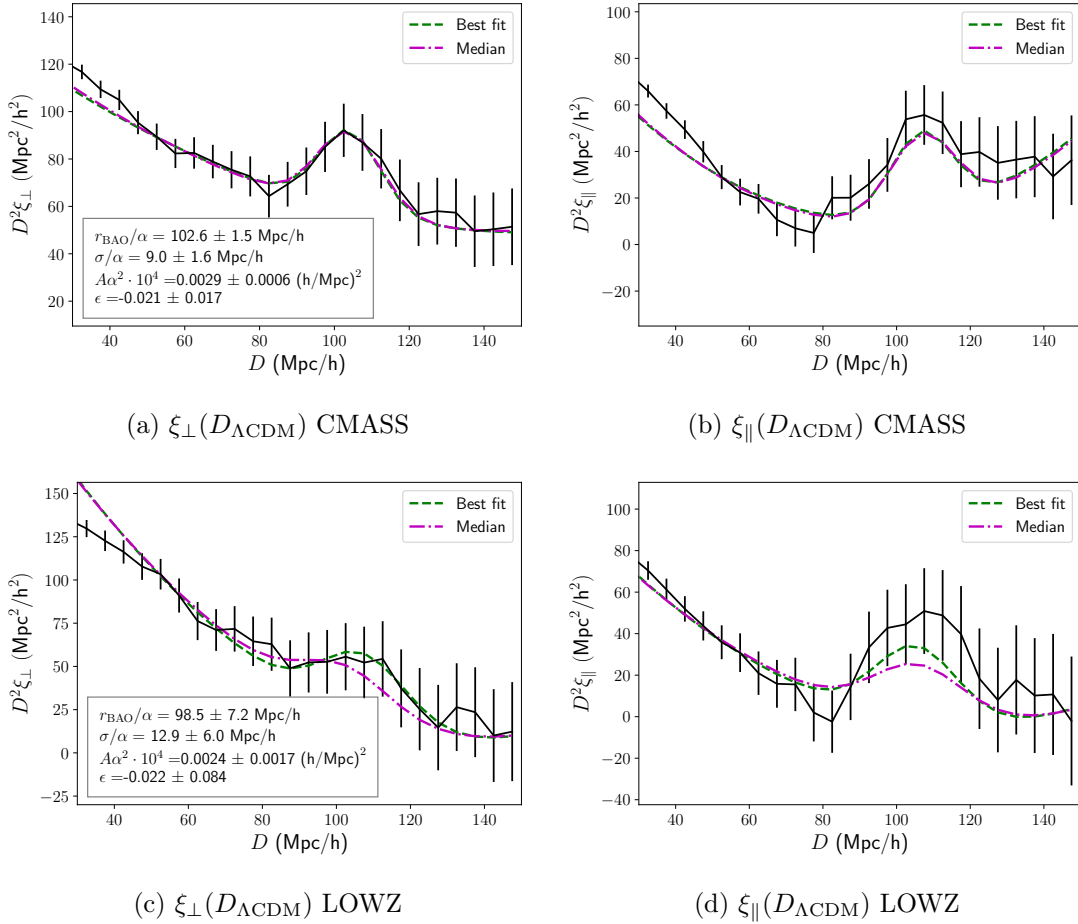


Figure 7: Combined fit to the transverse wedge $\xi_{\perp}(D_{\Lambda\text{CDM}})$ and radial wedge $\xi_{\parallel}(D_{\Lambda\text{CDM}})$ of the CMASS and LOWZ survey respectively, where $D_{\Lambda\text{CDM}}$ is the Lagrangian distance evaluated at present times for ΛCDM with $\Omega_{M0} = 0.3$. The model fit includes 10 parameters ($\frac{r_{\text{BAO}}}{\alpha}$, $\frac{\sigma}{\alpha}$, $A\alpha^2$, ϵ , $\bar{C}_{0\perp}$, $\bar{C}_{1\perp}$, $\bar{C}_{2\perp}$, $\bar{C}_{0\parallel}$, $\bar{C}_{1\parallel}$, $\bar{C}_{2\parallel}$). The best fit (green line) is the fit that maximises the likelihood function. The median fit (purple line) is based on the 50% quantiles of the Bayesian posterior, resulting from conservative priors (meaning priors that span the significant volume of the likelihood). The numerical values superimposed on the plot of ξ_{\perp} are the mean values with 1σ equal tail credible intervals.

a relative angular and radial sense compared to the “true” underlying cosmology, to lowest order. Since ϵ is consistent with zero at the $< 2\sigma$ level for both timescape and ΛCDM in the above data analysis, both models are in agreement with no anisotropic distortion. We can formulate the $\epsilon = 0$ consistency test in terms of the effective metric combination $g_{\theta\theta}^{1/2}/g_{zz}^{1/2}$ (equal to $d_A H/c$ in ΛCDM , where d_A is the angular diameter distance, and H is the Hubble parameter), which from the AP-scaling of our results can be formulated as

$$\frac{g_{\theta\theta}^{1/2}}{g_{zz}^{1/2}} \approx \frac{\alpha_{\perp}}{\alpha_{\parallel}} \frac{g_{\text{fid},\theta\theta}^{1/2}}{g_{\text{fid},zz}^{1/2}} = (1 + \epsilon)^{-3} \frac{g_{\text{fid},\theta\theta}^{1/2}}{g_{\text{fid},zz}^{1/2}} \quad (5.3)$$

where g_{fid} corresponds to the fiducial adapted metric of either ΛCDM or timescape, and

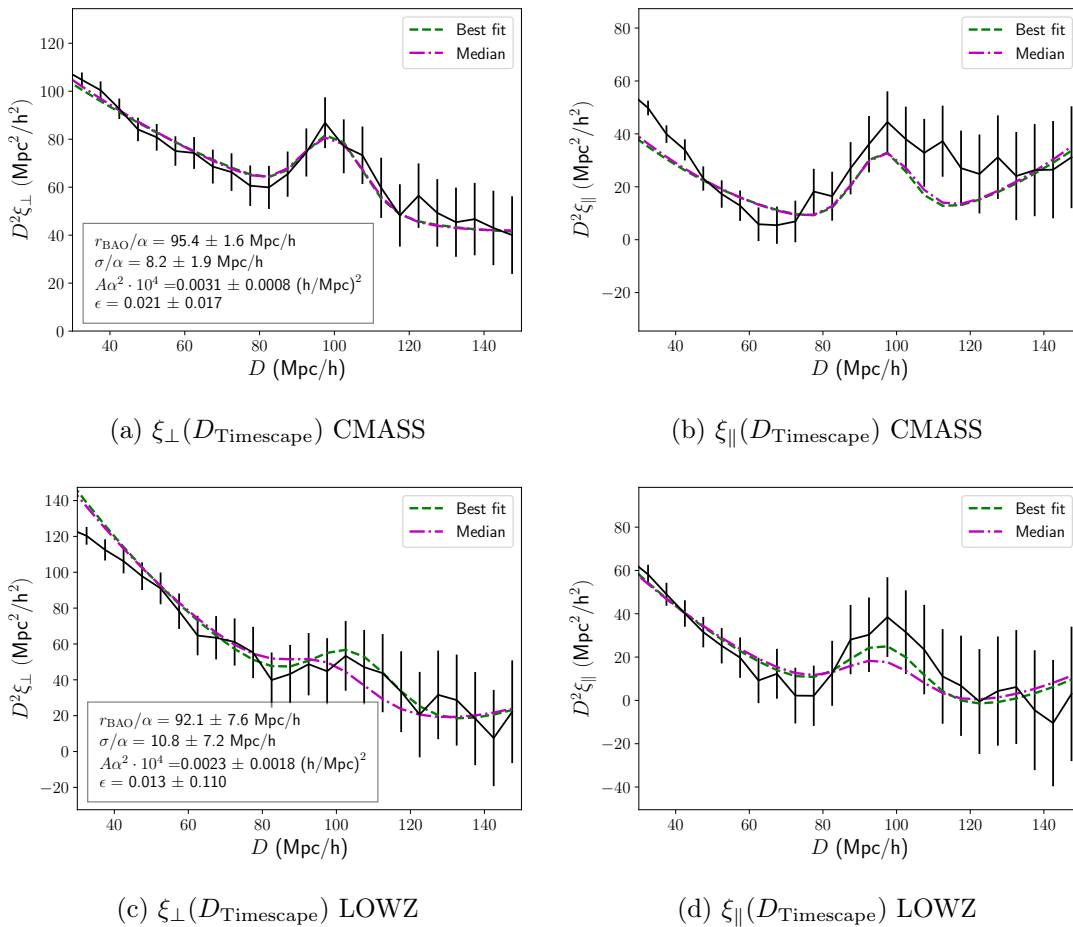


Figure 8: Combined fit to the transverse wedge $\xi_{\perp}(D_{\text{Timescape}})$ and radial wedge $\xi_{\parallel}(D_{\text{Timescape}})$ of the CMASS and LOWZ survey respectively, where $D_{\text{Timescape}}$ is the Lagrangian distance evaluated at present times for the timescape model with $\Omega_{M0} = 0.3$. The model fit includes 10 parameters ($\frac{r_{\text{BAO}}}{\alpha}$, $\frac{\sigma}{\alpha}$, $A\alpha^2$, ϵ , $\bar{C}_{0\perp}$, $\bar{C}_{1\perp}$, $\bar{C}_{2\perp}$, $\bar{C}_{0\parallel}$, $\bar{C}_{1\parallel}$, $\bar{C}_{2\parallel}$). The best fit (green line) is the fit that maximises the likelihood function. The median fit (purple line) is based on the 50% quantiles of the Bayesian posterior, resulting from conservative priors (meaning priors that span the significant volume of the likelihood). The numerical values superimposed on the plot of ξ_{\perp} are the mean values with 1σ equal tail credible intervals.

where ϵ is the estimate quoted in table 2 for the respective fiducial cosmologies. The results of the effective measurement of the metric combinations (5.3) for CMASS and LOWZ are shown in figure 9. We see that both effective measurements are consistent with the respective fiducial lines, as expected since the estimated ϵ -parameter is consistent with zero within both models. The precision in the measurements of the metric combination is comparable to the difference between the fiducial metric combination of the two cosmologies for the CMASS survey, potentially making this metric combination a useful discriminator between the Λ CDM and timescape model for future surveys. We also note that the systematics in the measurement arising from the choice of fiducial cosmology is of order the distance between the cosmologies, indicating that a careful analysis of the regime of application of the AP-scaling is needed.

Wedge fit $\xi_{\perp}, \xi_{\parallel}$	$\alpha^2 A \cdot 10^4$	r_{BAO}/α	$\sigma_{\text{BAO}}/\alpha$	ϵ	χ^2/N_{dof}
$\Lambda\text{CDM CMSS}$	0.0029 ± 0.0006	102.6 ± 1.5	9.0 ± 1.6	-0.021 ± 0.017	48/30
$\Lambda\text{CDM LOWZ}$	0.0024 ± 0.0017	98.5 ± 7.2	12.9 ± 6.0	-0.022 ± 0.084	40/30
Timescape CMSS	0.0031 ± 0.0008	95.4 ± 1.6	8.2 ± 1.9	0.021 ± 0.017	49/30
Timescape LOWZ	0.0023 ± 0.0018	92.1 ± 7.6	10.8 ± 7.2	0.013 ± 0.110	38/30
$\Lambda\text{CDM CMSS } \mathcal{N}_{\sigma_{\text{BAO}}/\alpha}$	0.0035 ± 0.0006	100.9 ± 1.8	12.3 ± 0.2	-0.022 ± 0.023	48/30
$\Lambda\text{CDM LOWZ } \mathcal{N}_{\sigma_{\text{BAO}}/\alpha}$	0.0027 ± 0.0012	100.3 ± 4.6	12.3 ± 0.3	-0.008 ± 0.060	40/30

Table 2: Results of the combined fit to the transverse and radial wedge for CMSS and LOWZ. The parameter estimates shown are the Bayesian median with 1σ equal tail credible intervals. Conservative priors (meaning priors that span the significant volume of the likelihood) are used for all parameters in all fits, except for the ΛCDM fits labelled $\mathcal{N}_{\sigma_{\text{BAO}}/\alpha}$, where a narrow Gaussian prior is used with mean and width as determined in the mock analysis of section 4.2. The minimum χ^2 value divided by number of degrees of freedom N_{dof} is also quoted. r_{BAO}/α and $\sigma_{\text{BAO}}/\alpha$ are in units of Mpc/h . A is in units of $(\text{Mpc}/h)^2$.

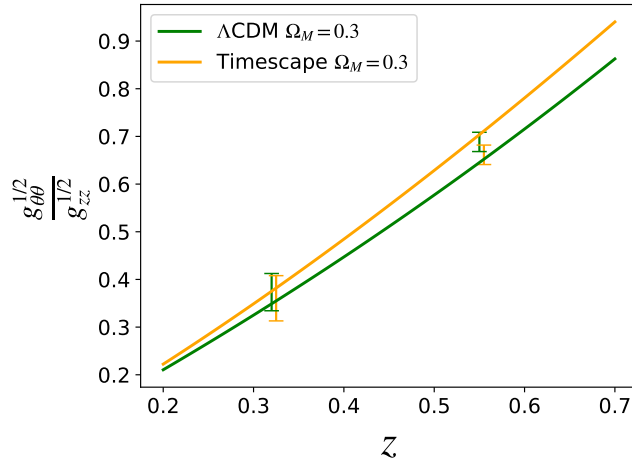


Figure 9: Effective measurement of the metric combination $g_{\theta\theta}^{1/2}/g_{zz}^{1/2}$ for LOWZ and CMSS within the timescape model and ΛCDM respectively, with the fiducial ΛCDM and timescape $\Omega_{M0} = 0.3$ predictions superimposed. The timescape measurements are artificially shifted slightly in redshift relative to the mean LOWZ and CMSS redshifts $z = 0.32$ and $z = 0.55$, in order to see the measurements and their comparison more clearly.

6 Discussion

In this paper we have developed methods for examining BAO features in the 2-point correlation function for cosmological models with non-trivial curvature: models that are not necessarily spatially flat, close to spatially flat, nor with constant spatial curvature. The methods outlined in section 2 and 4.1 are applicable for a broad class of large-scale cosmological models. (See section 2.2 for precise statements about the regime of applicability.) Our assumptions on the model cosmology can be summarised as follows:

- We assume global hyperbolicity of the average space-time, and that the galaxies can to a good approximation be described as particles in a non-caustic, vorticity-free fluid

description. These assumptions are made in order to formulate the reduced 2-point correlation function descriptive statistic in terms of the Lagrangian distance definition given in section 2.1, generalising the comoving distance definition of FLRW cosmology.

- We further impose the assumptions outlined in section 2.2, such that the Lagrangian distance definition can be approximated as in eq. (2.7). The approximation (2.7) is needed to: (i) define the “radial fraction” of the separation μ_T in (2.8); and (ii) make sense of the generalised AP-scalings $\alpha_{\parallel}, \alpha_{\perp}$ of the “radial” and “transverse” component of the metric introduced in section 2.3.
- Finally, we assume that the empirical fitting function described in section 4.1 is appropriate for extracting the isotropic BAO characteristic scale and the anisotropic distortion between the radial and transverse scale. (This assumption is tested and confirmed for a fiducial Λ CDM model using mocks catalogues, but is left as an ansatz for other cosmologies.)

Our methods allow us to explicitly formulate the 2-point correlation function in the context of a broad class of cosmologies and hence analyse the clustering statistics for those cosmologies in detail, instead of relying on results extrapolated from Λ CDM. The only Λ CDM estimate used in this paper enters when estimating errors in the observed 2-point correlation function, where we use mocks generated from a fiducial Λ CDM model to give a rough estimate for the variance over ensembles of our sky.

When testing our methods on Λ CDM mocks we recover the isotropic peak position to within one per cent of the fiducial value. This $\lesssim 1\%$ discrepancy is due to a calibration issue between the characteristic scale extracted in the fitting procedure and the underlying BAO scale discussed in section 4. It should be noted that, while this level of systematic error is somewhat higher than obtained by Λ CDM fitting procedures, it can be considered low in (semi-)model independent analysis. Removing cosmology dependence in data reduction necessarily comes at the price of increasing uncertainties. The systematics related to the BAO scale extraction in the context of other models must be assessed for each cosmology of interest. The anisotropic scaling parameter ϵ is recovered to high precision; the systematics in our mock analysis on the determination of ϵ are much smaller than the usual statistical errors in Λ CDM fitting procedures. The estimation of the ϵ parameter is robust to the exact form of the fitting function assumed, and is not associated with the calibration issues of the statistical BAO scale.

A shortcoming of this analysis is that a fiducial cosmology of choice is still needed in order to reduce data into a 2-point correlation function. Model-independent analysis has been proposed in, e.g., [45] and [46]. While such procedures are certainly relevant for next-generation surveys, the signal strength is greatly reduced due to the split of the fiducial spatial scale to a range of angular and redshift separations.

Another shortcoming of this paper is the approximations of section 2.2, implying that only effective cosmic metric theories which are averaged on scales of the order of the BAO scale can be tested in our framework. While testing more complicated models with a hierarchy of curvature scales, describing different scales of structure in our universe, would be of interest, this is beyond the scope of this paper.

We apply our fitting methods to the BOSS DR12 CMASS and LOWZ galaxy surveys using two fiducial cosmologies: a spatially flat Λ CDM model and the timescape model, which at the present epoch has a marginal apparent acceleration with a recent expansion history

closer to the empty FLRW universe. We recover the pre-reconstruction results for the BAO peak position and the anisotropic distortion parameter ϵ based on Λ CDM template-fitting obtained in [25].

It should be noted, that since the parameter estimates of our empirical procedure and of the standard Λ CDM template-fitting are based on the same datasets, any difference in the results can be attributed to systematic differences in the parameter extraction procedures. For procedures with small systematic differences as compared to the statistical errors, we would thus expect differences in parameter estimates much smaller than 1σ . The systematic differences between the present procedure and the standard Λ CDM procedure are smaller, but of order, the statistical errors. The main difference between the estimated BAO peak position of the present procedure and of the standard Λ CDM power spectrum fitting procedure can be ascribed to the systematics related to the calibration of the BAO scale in the empirical fit (see discussion in section 4). Other examples of systematics between the procedures that can lead to differences in the parameter estimates are: choice of statistical framework, choice of priors, and galaxy weights. For example, the $\sigma_{\text{BAO}}/\alpha$ prior in the present analysis has a $\sim 1\%$ effect on the peak position, which is comparable to the differences in our inferred scale as compared to the results of [25].

Based on our empirical model for the shape of the 2-point correlation function, we find that the BAO feature of the models is detected at a similar level of significance in the two cosmologies, and that the distortion between the radial and transverse directions, quantified by the ϵ parameter, is consistent with zero for both fiducial models within 2σ . Thus, both models are consistent with no anisotropic distortion with respect to the “true” cosmological model, and thus provide self-consistent fits to the BAO-data. This finding is interesting in light of the significant difference between the timescape model and the Λ CDM model distance measures (see figure 1).

Our analysis suggests that a wide class of cosmological models can yield a statistically isotropic BAO feature with $\epsilon = 0$, consistent with the expectation of statistical homogeneity and isotropy of our universe. In future work, we will combine these BAO measurements with estimations of the standard ruler scale in timescape cosmology to perform a full model comparison.

Acknowledgments

We wish to thank Thomas Buchert for hospitality at the ENS, Lyon, France. This work was supported by Catalyst grant CSG-UOC1603 administered by the Royal Society of New Zealand. AH is grateful for the support given by the funds: ‘Knud Højgaard’s Fond’, ‘Torben og Alice Frimodts Fond’, and ‘Max Nørgaard og Hustru Magda Nørgaard’s Fond’.

A Taylor expansion of geodesic distances

In the present analysis we make use of a Taylor expansion of the spatial geodesic distance between two points on a spatial hypersurface. Such an expansion is convenient when the spatial geodesic equation (defined on spatial hypersurfaces of interest) of the model under investigation has no analytic solution, and applicable when the curvature scale of the model is much larger than the particle separation of interest.

We consider a metric on the form eq. (2.1)

$$ds^2 = -\alpha^2 c^2 dt^2 + g_{ij} dx^i dx^j, \quad (\text{A.1})$$

where t defines a spatial foliation of interest. (In the context of this analysis, $t = \text{constant}$ slices are taken to coincide with the matter frame, which can be done in the absence of vorticity.)

Consider a geodesic spatial line between two points P_1 and P_2 on the hypersurface $t = T$, such that the line is required to lie in the $t = T$ plane everywhere. The geodesic distance between the points is given by

$$d_T(P_1, P_2) \equiv \int_{l_1}^{l_2} dl \sqrt{g_{ij} \frac{dx^i}{dl} \frac{dx^j}{dl}} = l_2 - l_1 \quad (\text{A.2})$$

where l is the affine parameter along a spatial geodesic connecting P_1 and P_2 , $\frac{dx^i}{dl}$ is the tangent to the geodesic with $g_{ij} \frac{dx^i}{dl} \frac{dx^j}{dl} = 1$, $l_1 = l(P_1)$ and $l_2 = l(P_2)$ is the affine parameter evaluated at the endpoints. The function d_T coincides with the Lagrangian distance D_T defined in section (2.1), when the points P_1 and P_2 represent the intersection of two particle worldlines with the surface $t = T$.

We expand the coordinate functions on the line in the affine parameter l

$$\begin{aligned} x_2^i &= x_1^i + \left. \frac{dx^i}{dl} \right|_{l=l_1} (l_2 - l_1) + f^i, \\ f^i &= \sum_{n=2}^{\infty} f_n^i, \quad f_n^i = \left. \frac{1}{n!} \frac{d^n x^i}{dl^n} \right|_{l=l_1} (l_2 - l_1)^n \end{aligned} \quad (\text{A.3})$$

where $x_1^i = x^i(P_1)$ and $x_2^i = x^i(P_2)$ are the coordinate labels of the end points. The higher-order terms f_n^i can be expressed in terms of $\Delta x^i = x_2^i - x_1^i$ up to a given order. Here we shall keep terms up to $\mathcal{O}(f_3^i)$, where we assume $\Delta x^j f_2^k \sim \mathcal{O}(f_3^i)$ etc. The second order term yields

$$\begin{aligned} f_2^i &= \frac{1}{2} \frac{d^2 x^i}{dl^2} (l_2 - l_1)^2 = -\frac{1}{2} \Gamma_{jk}^i \frac{dx^j}{dl} \frac{dx^k}{dl} (l_2 - l_1)^2 \\ &= -\frac{1}{2} \Gamma_{jk}^i (\Delta x^j - f^j) (\Delta x^k - f^k) = -\frac{1}{2} \Gamma_{jk}^i \Delta x^j \Delta x^k + \Gamma_{jk}^i \Delta x^j f_2^k + \mathcal{O}(f_4^i) \\ &= -\frac{1}{2} \Gamma_{jk}^i \Delta x^j \Delta x^k - \frac{1}{2} \Gamma_{jk}^i \Gamma_{st}^k \Delta x^j \Delta x^s \Delta x^t + \mathcal{O}(f_4^i), \end{aligned} \quad (\text{A.4})$$

where the first line follows from the affine geodesic equation, the second line follows from applying (A.3) and keeping terms up to $\mathcal{O}(f_3^i)$. The third line comes from recursively plugging (A.4) into itself and again keeping terms up to $\mathcal{O}(f_3^i)$. The evaluation at $l = l_1$ is implicit.

With a similar derivation, the third-order term of the expansion eq. (A.3) yields

$$f_3^i = \left(\frac{1}{3} \Gamma_{jk}^i \Gamma_{st}^k - \frac{1}{6} \partial_s \Gamma_{jt}^i \right) \Delta x^j \Delta x^s \Delta x^t + \mathcal{O}(f_4^i). \quad (\text{A.5})$$

We can now expand the geodesic distance (A.2) in an adapted coordinate system x^i of choice. Keeping terms up to $\mathcal{O}(f_4^i)$ we have

$$\begin{aligned} d_T(P_1, P_2) &= l_2 - l_1 = \sqrt{g_{ij} \frac{dx^i}{dl} \frac{dx^j}{dl}} (l_2 - l_1)^2 \\ &= \sqrt{g_{ij} (\Delta x^i - f^i) (\Delta x^j - f^j)} \\ &= \sqrt{g_{ij} \Delta x^i \Delta x^j - 2g_{ij} \Delta x^i (f_2^j + f_3^j) + g_{ij} f_2^i f_2^j + \mathcal{O}(f_5^i)} \\ &= \sqrt{{}^{(0)}g + {}^{(1)}g + {}^{(2)}g + \mathcal{O}(f_5^i)}, \end{aligned} \quad (\text{A.6})$$

where all terms are evaluated at $l = l_1$. The first line follows from a convenient multiplication by $1 = \sqrt{g_{ij} \frac{dx^i}{dt} \frac{dx^j}{dt}}$. The following lines come from applying the expansion (A.3) and truncating the resulting terms at $\mathcal{O}(f_4^i)$. In the last line we have used the definitions

$$\begin{aligned} {}^{(0)}g &\equiv g_{ij} \Delta x^i \Delta x^j, & {}^{(1)}g &\equiv g_{ij} \Gamma_{st}^j \Delta x^i \Delta x^s \Delta x^t \\ {}^{(2)}g &\equiv \left[\frac{1}{3} g_{ij} \left(\partial_s \Gamma_{tb}^j + \Gamma_{ab}^j \Gamma_{st}^a \right) + \frac{1}{4} g_{kj} \Gamma_{st}^k \Gamma_{ib}^j \right] \Delta x^i \Delta x^s \Delta x^t \Delta x^b \end{aligned} \quad (\text{A.7})$$

The extent to which the coordinate expansion (A.6) is accurate at a given truncation of the series depends on the space-time metric and the chosen events P_1 and P_2 , but also on the adapted coordinates used in the expansion. The convergence of the expansion (A.6) must be examined for the particular problem at hand.

A.1 Spherically symmetric metrics

As a special case relevant for this paper we consider the spherically-symmetric metric (2.3) of section 2.2. The adapted metric on the spatial hypersurfaces given by eq. (2.4)

$$ds_T^2 = g_{rr}(t = T, r) dr^2 + g_{\theta\theta}(t = T, r) (d\theta^2 + \cos^2(\theta) d\phi^2). \quad (\text{A.8})$$

In this case we have for the lowest-order term of eq. (A.6)

$${}^{(0)}g = g_{rr}(\Delta r)^2 + g_{\theta\theta} ((\Delta\theta)^2 + \cos^2(\theta)(\Delta\phi)^2). \quad (\text{A.9})$$

The first order correction yields

$$\begin{aligned} {}^{(1)}g &= \frac{1}{2} \frac{\partial}{\partial x^k} (g_{sm}) \Delta x^m \Delta x^k \Delta x^s \\ &= \frac{1}{2} \Delta g_{rr} (\Delta r)^2 + \frac{1}{2} \Delta g_{\theta\theta} ((\Delta\theta)^2 + \cos^2(\theta)(\Delta\phi)^2) + \frac{1}{2} g_{\theta\theta} [\Delta \cos^2(\theta)] (\Delta\phi)^2, \end{aligned} \quad (\text{A.10})$$

where we have defined

$$\Delta g_{rr} \equiv \frac{dg_{rr}}{dr} \Delta r, \quad \Delta g_{\theta\theta} \equiv \frac{dg_{\theta\theta}}{dr} \Delta r, \quad \Delta \cos^2(\theta) \equiv \frac{d(\cos^2(\theta))}{d\theta} \Delta\theta. \quad (\text{A.11})$$

Combining the lowest order term and the first order correction we thus have for eq. (A.6) up to $\mathcal{O}({}^{(2)}g)$

$$d_T(P_1, P_2) = \sqrt{\bar{g}_{rr}(\Delta r)^2 + \bar{g}_{\theta\theta} \left((\Delta\theta)^2 + \overline{\cos^2(\theta)} (\Delta\phi)^2 \right)} + \mathcal{O}({}^{(2)}g), \quad (\text{A.12})$$

where we have used the definition

$$\bar{g}_{rr} \equiv g_{rr} + \frac{1}{2} \Delta g_{rr}, \quad \bar{g}_{\theta\theta} \equiv g_{\theta\theta} + \frac{1}{2} \Delta g_{\theta\theta}, \quad \overline{\cos^2(\theta)} \equiv \cos^2(\theta) + \frac{1}{2} \Delta \cos^2(\theta), \quad (\text{A.13})$$

and a term $-\frac{1}{2} \Delta g_{\theta\theta} [\Delta \cos^2(\theta)] (\Delta\phi)^2$ is subsumed in the $\mathcal{O}({}^{(2)}g)$ terms in (A.12). Hence the first order correction represents a shift of evaluation at x_1^i to the mean coordinate point $\bar{x}^i = x_1^i + \frac{1}{2} \Delta x^i$.

We can examine the accuracy of the approximation (A.12), truncated at first order, by evaluating the second order correction terms of ${}^{(2)}g$, which will contain terms of order $\sim \frac{({}^{(1)}g)^2}{({}^{(0)}g)}$ and terms involving the second derivatives of the metric. All of these terms should be evaluated in the model of interest and in the desired coordinate system, in order to examine the approximation (A.12). For observational coordinates (z, θ, ϕ) in both the FLRW and timescape model with realistic model parameters, we find $\frac{({}^{(2)}g)}{({}^{(0)}g)} \lesssim 10^{-3}$, for separation distances $\Delta z, \Delta\theta, \Delta\phi$ around the BAO scale.

B The 2-point correlation function

The spatial 2-point correlation function ξ describes the excess probability of finding two galaxies at two given points on a spatial surface, relative to an uncorrelated sample. The typical formulation of the 2-point correlation function in standard cosmology is tightly linked to the assumption of symmetries of the “background” FLRW space-time, and the ergodic assumptions on the density perturbation field on top of the background, which leads to the modelling of the galaxy distribution as a stationary and ergodic point process.

Thus if we revisit the “background” cosmology, or do cosmology without imposing a background, we should also revisit the theory underlying the 2-point correlation function. Here we seek to provide a more general introduction to the 2-point correlation function, valid for models with no exact symmetries in the pointwise ensemble average of the galaxy counts.

Consider a spatial domain of a hypersurface \mathcal{D} . We view the position of the galaxies within this domain as random variables, and fix the total number of galaxies N within the domain \mathcal{D} . We use adapted coordinates x^i on the hypersurface, and denote the random position of the a 'th particle x_a^i . The scaled probability (ensemble average number count) of finding two galaxies located in the infinitesimal volume elements dV_X and dV_Y centred at the points $x^i = X^i$ and $x^i = Y^i$ can be written as

$$f(X, Y)dV_X dV_Y \equiv \langle N(dV_X)N(dV_Y) \rangle, \quad (\text{B.1})$$

where $f(X, Y)$ is the number count density and where

$$N(dV_X) \equiv \sum_a^N \mathbb{1}_{dV_X}(x_a^i). \quad (\text{B.2})$$

is the number count in the volume element dV_X in a given realisation, where

$$\mathbb{1}_{dV_X}(x_a^i) = \begin{cases} 1, & x_a^i \in dV_X, \\ 0, & x_a^i \notin dV_X, \end{cases} \quad (\text{B.3})$$

is the indicator function. (If the volume dV_X is made small enough, this is zero or one in practice.) The spatial volume elements dV are given by¹⁶ the adapted metric (2.1)

$$dV = \sqrt{\det(g_{ij})} dx^1 \wedge dx^2 \wedge dx^3. \quad (\text{B.4})$$

The integral of (B.1) over two arbitrary domains $\mathcal{D}_X \in \mathcal{D}$ and $\mathcal{D}_Y \in \mathcal{D}$ is

$$\int_{X \in \mathcal{D}_X} \int_{Y \in \mathcal{D}_Y} f(X, Y)dV_X dV_Y = \langle N(\mathcal{D}_X)N(\mathcal{D}_Y) \rangle \quad (\text{B.5})$$

following from the property $\mathbb{1}_{A \cup B}(y) = \mathbb{1}_A(y) + \mathbb{1}_B(y)$ of the indicator function, where A and B are disjoint sets.

The scaled probability of finding a galaxy in the small volume dV_X (ensemble average number count) can be expressed as an integral over (B.5)

$$f(X)dV_X \equiv \langle N(dV_X) \rangle = \frac{1}{N} \int_{Y \in \mathcal{D}} f(X, Y)dV_X dV_Y. \quad (\text{B.6})$$

¹⁶We could alternatively absorb any non-zero function into the number count density $f(X, Y)$ and make the redefinition $f(X, Y) \rightarrow \det(g_{ij})f(X, Y)$, $dV \rightarrow dV/\sqrt{\det(g_{ij})} = dx^1 \wedge dx^2 \wedge dx^3$ if we prefer to work in terms of coordinate volumes instead of physical volumes.

We shall be interested in writing the probability (B.1) in terms of the excess probability of the uncorrelated process

$$f_{\text{Poisson}}(X, Y) = f(X)f(Y), \quad X \neq Y. \quad (\text{B.7})$$

Assuming that $f(X) \neq 0$ over the domain \mathcal{D} we can write

$$f(X, Y) dV_X dV_Y = f(X)f(Y) (1 + \xi(X, Y)) dV_X dV_Y \quad (\text{B.8})$$

where we have defined

$$\xi(X, Y) = \frac{f(X, Y)}{f(X)f(Y)} - 1. \quad (\text{B.9})$$

This correlation function, ξ , is zero for $X \neq Y$ for a Poisson point process per construction, and measures the departure from an uncorrelated distribution of galaxies.

The correlation function (B.9) is a function of all 6 variables (X^i, Y^i) in a general inhomogeneous universe. In practice, in BAO analysis, we are interested in integrating out some of these degrees of freedom, to isolate a characteristic statistical scale. We can make the substitution $(X^i, Y^i) \rightarrow (X^i, \hat{n}_X^i, D)$ in (B.1), where \hat{n}_X^i is a unit vector at X^i defining a geodesic starting at X^i and intersecting Y^i and D is the geodesic distance from X^i to Y^i

$$f(X, Y) dV_X dV_Y = f(X, \hat{n}_X, D) dV_X d\hat{n}_X dD = f(X, \hat{n}_X, D) J dV_X dV_Y \quad (\text{B.10})$$

with

$$J \equiv \det \left(\frac{\partial(X, \hat{n}_X, D)}{\partial(X, Y)} \right) \quad (\text{B.11})$$

being the Jacobian of the transformation. It follows that (B.9) reads

$$\xi(X, \hat{n}_X, D) = \frac{f(X, \hat{n}_X, D)}{f_{\text{Poisson}}(X, \hat{n}_X, D)} - 1, \quad (\text{B.12})$$

where the Jacobian J of the transformation $(X^i, Y^i) \rightarrow (X^i, \hat{n}_X^i, D)$ cancels in (B.9), since f and f_{Poisson} have identical transformations. We denote the random process underlying the ensemble homogeneous and isotropic if $f_{HI}(X + \alpha) = f_{HI}(X)$, $f_{HI}(X + \alpha, R\hat{n}_X, D) = f_{HI}(X, \hat{n}_X, D)$ are satisfied, where α is an arbitrary translation, R is an arbitrary rotation of the unit vector \hat{n}_X , and where the subscript HI stands for homogenous and isotropic. In this case (B.12) becomes the so-called reduced 2-point correlation function

$$\xi_{HI}(D) = \frac{f_{HI}(D)}{f_{HI \text{ Poisson}}(D)} - 1. \quad (\text{B.13})$$

In the general case where the random process underlying the ensemble is not associated with any exact symmetries, we can still create a reduced version of the correlation function (B.12) by marginalising over the direction and position degrees of freedom \hat{n}_X, X . This can be done as follows. We define the marginalised number count density over a subdomain $\mathcal{D}_S \in \mathcal{D}$ as

$$f(D, \mathcal{D}_S) \equiv \int_{X \in \mathcal{D}_S} dV_X \int dn_X f(X, \hat{n}_X, D). \quad (\text{B.14})$$

The marginalised ensemble number count in a small range of affine distance dD is given by

$$f(D, \mathcal{D}_S) dD = \left\langle \sum_{a,b}^N \mathbb{1}_{[D, D+dD]}(D(x_a^i, x_b^i)) \mathbb{1}_{\mathcal{D}_S}(x_a^i) \right\rangle, \quad (\text{B.15})$$

where we have used the fact that we can rewrite the number count in terms of the new coordinates X, \hat{n}_X, D ,

$$\begin{aligned} N(dV_X)N(dV_Y) &= \sum_{a,b}^N \mathbb{1}_{dV_X}(x_a^i) \mathbb{1}_{dV_Y}(x_b^i) \\ &= \sum_{a,b}^N \mathbb{1}_{dV_X}(x_a^i) \mathbb{1}_{[\hat{n}_X, \hat{n}_X+d\hat{n}_X]}(\hat{n}_X(x_a^i, x_b^i)) \mathbb{1}_{[D, D+dD]}(D(x_a^i, x_b^i)), \end{aligned} \quad (\text{B.16})$$

and that by (B.10) $f(X, \hat{n}_X, D) dV_X d\hat{n}_X dD = \langle N(dV_X)N(dV_Y) \rangle$. We can write (B.14) in terms of $f_{\text{Poisson}}(D, \mathcal{D}_S)$ defined through the integral over $f_{\text{Poisson}}(X, \hat{n}_X, D)$ analogous to (B.14).

$$f(D, \mathcal{D}_S) dD = f_{\text{Poisson}}(D, \mathcal{D}_S) (1 + \xi(D, \mathcal{D}_S)) dD, \quad (\text{B.17})$$

with

$$\xi(D, \mathcal{D}_S) = \frac{f(D, \mathcal{D}_S)}{f_{\text{Poisson}}(D, \mathcal{D}_S)} - 1, \quad (\text{B.18})$$

which we denote the ‘‘marginalised’’ two point correlation function.

Note that eq. (B.18) has the form of the conventional reduced 2-point correlation function of a homogenous and isotropic cosmology. However, the interpretation is different here, as the reduction does not follow from symmetry assumptions on the probability distribution of the density field, but rather follows from marginalisation over the position and direction degrees of freedom (and hence depends on scale through \mathcal{D}_S). Eq. (B.18) coincides with the conventional 2-point correlation function (B.13) when the galaxy distribution is assumed to be represented by a homogeneous and isotropic point process. We can thus view eq. (B.18) as a generalisation of the 2-point correlation function to inhomogeneous space-times.

For models of the form outlined in section 2.2 we can decompose \hat{n}_X into $\mu, \text{sgn}(\delta z)$, and the normalised angular separation vector $\delta\hat{\Theta} = \frac{1}{|\delta\Theta|}(\delta\theta, \cos(\theta)\delta\phi)$. In this case we can write

$$f(X, Y) dV_X dV_Y = f(X, \mu, \text{sgn}(\delta z), \delta\hat{\Theta}, D) dV_X d\mu d\delta\hat{\Theta} dD \quad (\text{B.19})$$

and we can construct a marginalised number count density in D analogous to (B.14) by marginalising over the remaining variables. We shall sometimes be interested in keeping μ as a variable, and construct the following marginalised number count density

$$f(D, \mu, \mathcal{D}_S) \equiv \sum_{\text{sgn}(\delta z)=\pm 1} \int_{X \in \mathcal{D}_S} dV_X \int d\delta\hat{\Theta} f(X, \mu, \text{sgn}(\delta z), \delta\hat{\Theta}, D), \quad (\text{B.20})$$

for which we can define the marginalised μ -dependent 2-point correlation function

$$\xi(D, \mu, \mathcal{D}_S) = \frac{f(D, \mu, \mathcal{D}_S)}{f_{\text{Poisson}}(D, \mu, \mathcal{D}_S)} - 1. \quad (\text{B.21})$$

Integrating out the μ -dependence in (B.20) we arrive at the marginalised isotropic number count density $f(D, \mathcal{D}_S)$ from which we can construct the isotropic marginalised 2-point correlation function of (B.18).¹⁷

We define the “wedge” as the mean of eq. (B.21) over a given μ range $[\mu_1, \mu_2]$.

$$\xi_{[\mu_1, \mu_2]}(D) \equiv \frac{1}{\mu_2 - \mu_1} \int_{\mu_1}^{\mu_2} d\mu \xi(D, \mu), \quad (\text{B.22})$$

where the dependence on \mathcal{D}_S is implicit in (B.22) and in the following. It can be viewed as the mean excess of probability of finding two galaxies a distance D apart over the given μ range. We define the transverse and the radial wedge as respectively

$$\xi_{\perp}(D) \equiv \xi_{[0, 0.5]}(D), \quad \xi_{\parallel}(D) \equiv \xi_{[0.5, 1]}(D). \quad (\text{B.23})$$

When $f(D, \mu)$ is mainly depending on D such that

$$\begin{aligned} f(D, \mu) &= f(D)(1 + h(D, \mu)), & h(D, \mu) &\ll 1 \\ f_{\text{Poisson}}(D, \mu) &= f_{\text{Poisson}}(D)(1 + h_{\text{Poisson}}(D, \mu)), & h_{\text{Poisson}}(D, \mu) &\ll 1, \end{aligned} \quad (\text{B.24})$$

we have the useful approximation

$$\begin{aligned} \int_0^1 d\mu \xi(D, \mu) &= \int_0^1 d\mu \frac{f(D)(1 + h(D, \mu))}{f_{\text{Poisson}}(D)(1 + h_{\text{Poisson}}(D, \mu))} - 1 \\ &\approx \int_0^1 d\mu \frac{f(D)}{f_{\text{Poisson}}(D)} (1 + h(D, \mu) - h_{\text{Poisson}}(D, \mu)) - 1 \\ &= \frac{f(D)}{f_{\text{Poisson}}(D)} - 1 = \xi(D) \end{aligned} \quad (\text{B.25})$$

where we have used $\int_0^1 d\mu h(D, \mu) = 0$ and $\int_0^1 d\mu h_{\text{Poisson}}(D, \mu) = 0$ by construction. Note that corrections to eq. (B.25) are *second order* in h and h_{Poisson} . A similar approximation can be formulated for the wedges (B.22)

$$\xi_{[\mu_1, \mu_2]}(D) \approx \xi(D, \mu_1 \leq \mu \leq \mu_2) \equiv \frac{f(D, \mu_1 \leq \mu \leq \mu_2)}{f_{\text{Poisson}}(D, \mu_1 \leq \mu \leq \mu_2)} - 1. \quad (\text{B.26})$$

References

- [1] P.J.E. Peebles and J.T. Yu, *Primeval Adiabatic Perturbation in an Expanding Universe*, *Astrophys. J.* **162** (1970) 815.
- [2] R.A. Sunyaev and Ya.B. Zeldovich, *Small-Scale Fluctuations of Relic Radiation*, *Astrophys. Space Sci.* **7** (1970) 3.
- [3] D.J. Eisenstein and W. Hu, *Baryonic Features in the Matter Transfer Function*, *Astrophys. J.* **496** (1198) 605, [[astro-ph/9709112](#)]

¹⁷For the estimate of (B.21) or (B.18) based on number counts in a subdomain $\mathcal{D}_{S'}$ of a single realisation of the ensemble to be representative for the ensemble average, we must invoke the approximate convergence condition $\hat{\xi}(D, \mathcal{D}_{S'})_{\lim V(\mathcal{D}_{S'}) \rightarrow \infty} \approx \xi(D, \mathcal{D}_S)$ for some choice of scale $V(\mathcal{D}_S)$, with fast enough convergence of the estimate. In practice $\mathcal{D}_{S'}$ will correspond to a given survey domain.

- [4] T. Matsubara, *Correlation Function in Deep Redshift Space as a Cosmological Probe*, *Astrophys. J.* **615** (2004) 573, [[astro-ph/0408349](#)]
- [5] S. Cole, et al., *The 2dF Galaxy Redshift Survey: Power-spectrum analysis of the final dataset and cosmological implications*, *Mon. Not. R. Astr. Soc.* **362** (2005) 505, [[astro-ph/0501174](#)]
- [6] D.J. Eisenstein, et al., *Detection of the Baryon Acoustic Peak in the Large-Scale Correlation Function of SDSS Luminous Red Galaxies*, *Astrophys. J.* **633** (2005) 560, [[astro-ph/0501171](#)]
- [7] C. Blake, E. Kazin, et al., *The WiggleZ Dark Energy Survey: mapping the distance-redshift relation with baryon acoustic oscillations*, *Mon. Not. R. Astr. Soc.* **418** (2011) 1707, [[arXiv:1108.2635](#)]
- [8] S. Alam, et al., *The clustering of galaxies in the completed SDSS-III Baryon Oscillation Spectroscopic Survey: cosmological analysis of the DR12 galaxy sample*, *Mon. Not. R. Astr. Soc.* **470** (2017) 2617, [[arXiv:1607.03155](#)]
- [9] N.G. Busca, et al., *Baryon acoustic oscillations in the Ly α forest of BOSS quasars*, *Astron. Astrophys.* **552** (2013) A96, [[arXiv:1211.2616](#)]
- [10] T. Delubac et al., *Baryon acoustic oscillations in the Ly α forest of BOSS DR11 quasars*, *Astron. Astrophys.* **574** (2015) A59, [[arXiv:1404.1801](#)]
- [11] N. Aghanim, et al., *Planck 2018 results. VI. Cosmological parameters*, [arXiv:1807.06209](#)
- [12] W.L. Freedman, *Cosmology at a Crossroads*, *Nature Astron.* **1** (2017) 0121, [[arXiv:1706.02739](#)]
- [13] P.A.R. Ade, et al., *Planck 2015 results. XXIV. Cosmology from Sunyaev-Zeldovich cluster counts*, *Astron. Astrophys.* **594** (2016) A24, [[arXiv:1502.01597](#)]
- [14] H. Hildebrandt, et al., *KiDS-450: Cosmological parameter constraints from tomographic weak gravitational lensing*, *Mon. Not. R. Astr. Soc.* **465** (2017) 1454, [[arXiv:1606.05338](#)]
- [15] H.M. Bourboux, et al., *Baryon acoustic oscillations from the complete SDSS-III Ly α -quasar cross-correlation function at $z=2.4$* , *Astron. Astrophys.* **608** (2017) A130, [[arXiv:1708.02225](#)]
- [16] B.D. Fields, *The primordial lithium problem*, *Ann. Rev. Nucl. Part. Sci.* **61** (2011) 47, [[arXiv:1203.3551](#)]
- [17] D.L. Wiltshire, *Cosmic clocks, cosmic variance and cosmic averages*, *New J. Phys.* **9** (2007) 377, [[arXiv:0702.0732](#)]
- [18] D.L. Wiltshire, *Exact solution to the averaging problem in cosmology*, *Phys. Rev. Lett.* **99** (2007) 251101, [[arXiv:0709.0732](#)]
- [19] M. Lavinto, S. Räsänen and S.J. Szybka, *Average expansion rate and light propagation in a cosmological Tardis spacetime*, *J. Cosmol. Astropart. Phys.* **12** (2013) 051, [[arXiv:1308.6731](#)]
- [20] T. Buchert, *On average properties of inhomogeneous fluids in general relativity. I: Dust cosmologies*, *Gen. Relativ. Grav.* **32** (2000) 105, [[gr-qc/9906015](#)]
- [21] T. Buchert and S. Räsänen, *Backreaction in late-time cosmology*, *Ann. Rev. Nucl. Part. Sci.* **62** (2012) 57, [[arXiv:1112.5335](#)]
- [22] D. Sapone, E. Majerotto and S. Nesseris, *Curvature versus distances: Testing the FLRW cosmology*, *Phys. Rev. D* **90** (2014) 023012, [[arXiv:1402.2236](#)]
- [23] D.L. Wiltshire, *Average observational quantities in the timescape cosmology*, *Phys. Rev. D* **80** (2009) 123512, [[arXiv:0909.0749](#)]
- [24] L. Anderson, E. Aubourg, et al., *The clustering of galaxies in the SDSS-III Baryon Oscillation Spectroscopic Survey: baryon acoustic oscillations in the Data Releases 10 and 11 Galaxy samples*, *Mon. Not. R. Astr. Soc.* **441** (2014) 24, [[arXiv:1312.4877](#)]

- [25] A.J. Cuesta, M. Vargas-Magaña, et al., *The clustering of galaxies in the SDSS-III Baryon Oscillation Spectroscopic Survey: Baryon Acoustic Oscillations in the correlation function of LOWZ and CMASS galaxies in Data Release 12*, *Mon. Not. R. Astr. Soc.* **457** (2016) 1770, [[arXiv:1509.06371](#)]
- [26] D.J. Eisenstein, H. Seo, E. Sirko and D. Spergel, *Improving Cosmological Distance Measurements by Reconstruction of the Baryon Acoustic Peak*, *Astrophys. J.* **664** (2007) 675, [[astro-ph/0604362](#)]
- [27] C. Blake, I. Achitouv, A. Burden and Y. Rasera, *The environmental dependence of the baryon acoustic peak in the Baryon Oscillation Spectroscopic Survey CMASS sample*, *Mon. Not. R. Astr. Soc.* **482** (2018) 578, [[arXiv:1810.01655](#)]
- [28] B.F. Roukema, T. Buchert, J.J. Ostrowski and M.J. France, *Evidence for an environment-dependent shift in the baryon acoustic oscillation peak*, *Mon. Not. R. Astr. Soc.* **448** (2015) 1660, [[arXiv:1410.1687](#)]
- [29] M.C. Neyrinck, et al., *Density-dependent clustering - I. Pulling back the curtains on motions of the BAO peak*, *Mon. Not. R. Astr. Soc.* **478** (2018) 2495, [[arXiv:1610.06215](#)]
- [30] X. Xu, A.J. Cuesta, N. Padmanabhan, D.J. Eisenstein and C.K. McBride, *Measuring D_A and H at $z = 0.35$ from the SDSS DR7 LRGs using baryon acoustic oscillations*, *Mon. Not. R. Astr. Soc.* **431** (2013) 2834, [[arXiv:1206.6732](#)]
- [31] S. Räsänen, *Light propagation in statistically homogeneous and isotropic dust universes*, *J. Cosmol. Astropart. Phys.* **03** (2010) 018, [[arXiv:0812.2872](#)]
- [32] D.L. Wiltshire, *Cosmic structure, averaging and dark energy*, in *Cosmology and Gravitation: Proc. XVth Brazilian School*, eds. M. Novello, and S.E. Perez Bergliaffa, (Cambridge Scientific Publishers, Cambridge, 2014) 203–244, [[arXiv:1311.3787](#)]
- [33] J.A.G. Duley, M.A. Nazer and D.L. Wiltshire, *Timescape cosmology with radiation fluid*, *Class. Quantum Grav.* **30** (2013) 175006, [[arXiv:1306.3208](#)]
- [34] M.A. Nazer and D.L. Wiltshire, *Cosmic microwave background anisotropies in the timescape cosmology*, *Phys. Rev. D* **91** (2015) 063519 [[arXiv:1410.3470](#)]
- [35] L.H. Dam, A. Heinesen and D.L. Wiltshire, *Apparent cosmic acceleration from type Ia supernovae*, *Mon. Not. R. Astr. Soc.* **472** (2017) 835, [[arXiv:1706.07236](#)]
- [36] P.J.E. Peebles, *Statistical Analysis of Catalogs of Extragalactic Objects. I. Theory*, *Astrophys. J.* **185** (1973) 413
- [37] M. Kerscher, I. Szapudi and A.S. Szalay, *A comparison of estimators for the two-point correlation function*, *Astrophys. J.* **535** (2000) L13, [[astro-ph/9912088](#)]
- [38] S.D. Landy and A.S. Szalay, *Bias and variance of angular correlation functions*, *Astrophys. J.* **412** (1993) 64
- [39] D.J. Eisenstein, et al., *SDSS-III: Massive Spectroscopic Surveys of the Distant Universe, the Milky Way, and Extra-Solar Planetary Systems*, *Astron. J.* **142** (2011) 72, [[arXiv:1101.1529](#)]
- [40] K.S. Dawson, et al., *The Baryon Oscillation Spectroscopic Survey of SDSS-III*, *Astron. J.* **145** (2013) 10, [[arXiv:1208.0022](#)]
- [41] S. Alam et al., *The Eleventh and Twelfth Data Releases of the Sloan Digital Sky Survey: Final Data from SDSS-III*, *Astrophys. J. Suppl.* **219** (2015) 12, [[arXiv:1501.00963](#)]
- [42] B. Reid, S. Ho, et al., *SDSS-III Baryon Oscillation Spectroscopic Survey Data Release 12: galaxy target selection and large scale structure catalogues*, *Mon. Not. R. Astr. Soc.* **455** (2016) 1553, [[arXiv:1509.06529](#)]
- [43] H.A. Feldman, N. Kaiser and J.A. Peacock, *Power spectrum analysis of three-dimensional redshift surveys*, *Astrophys. J.* **426** (1994) 23, [[astro-ph/9304022](#)]

- [44] M. Vargas-Magaña, S. Ho, et al., *The clustering of galaxies in the completed SDSS-III Baryon Oscillation Spectroscopic Survey: theoretical systematics and Baryon Acoustic Oscillations in the galaxy correlation function*, *Mon. Not. R. Astr. Soc.* **477** (2018) 1153, [[arXiv:1610.03506](#)]
- [45] E. Sanchez, D. Alonso, F.J. Sanchez, J.G.-Bellido and I. Sevilla, *Precise Measurement of the Radial Baryon Acoustic Oscillation Scales in Galaxy Redshift Surveys*, *Mon. Not. R. Astr. Soc.* **434** (2013) 2008, [[arXiv:1210.6446](#)]
- [46] E. Sanchez, A. Carnero, et al., *Tracing The Sound Horizon Scale With Photometric Redshift Surveys*, *Mon. Not. R. Astr. Soc.* **411** (2011) 277, [[arXiv:1006.3226](#)]
- [47] R.E. Smith, R. Scoccimarro and R.K. Sheth, *Motion of the acoustic peak in the correlation function*, *Phys. Rev. D* **77** (2008) 043525, [[astro-ph/0703620](#)]
- [48] H.-J. Seo, E.R. Siegel, D.J. Eisenstein and M. White, *Non-linear structure formation and the acoustic scale*, *Astrophys. J.* **686** (2008) 13, [[arXiv:0805.0117](#)]
- [49] K. Bolejko, M.A. Nazer and D.L. Wiltshire, *Differential cosmic expansion and the Hubble flow anisotropy*, *J. Cosmol. Astropart. Phys.* **06** (2016) 035, [[arXiv:1512.07364](#)]
- [50] L.H. Dam, *Inhomogeneous cosmological models and the cosmic microwave background*, M.Sc. thesis, (University of Canterbury, Christchurch, 2016), <http://hdl.handle.net/10092/13167>
- [51] N. Kaiser, *Clustering in real space and in redshift space*, *Mon. Not. R. Astr. Soc.* **227** (1987) 1.
- [52] M. White, M. Blanton, et al., *The clustering of massive galaxies at $z = 0.5$ from the first semester of BOSS data*, *Astrophys. J.* **728** (2011) 126, [[arXiv:1010.4915](#)]
- [53] C. Blake, et al., *The WiggleZ Dark Energy Survey: testing the cosmological model with baryon acoustic oscillations at $z = 0.6$* , *Mon. Not. R. Astr. Soc.* **415** (2011) 2892, [[arXiv:1105.2862](#)]
- [54] M. Davis and P.J.E. Peebles, *A survey of galaxy redshifts. V - The two-point position and velocity correlations*, *Astrophys. J.* **267** (1983) 465